IN-LB	Inch-Pound Units
SI	International System of Units

Form Pressure Exerted by Self-Consolidating Concrete: Primary Factors and Prediction Models—Report

Reported by ACI Committee 237

ACI PRC-237.2-21

American Concrete Institute
Always advancing

First Printing
July 2021
ISBN: 978-1-64195-145-6

Form Pressure Exerted by Self-Consolidating Concrete: Primary Factors and Prediction Models—Report

The technical committees responsible for ACI committee reports and standards strive to avoid ambiguities, omissions, and errors in these documents. In spite of these efforts, the users of ACI documents occasionally find information or requirements that may be subject to more than one interpretation or may be incomplete or incorrect. Users who have suggestions for the improvement of ACI documents are requested to contact ACI via the errata website at http://concrete.org/Publications/DocumentErrata.aspx. Proper use of this document includes periodically checking for errata for the most up-to-date revisions.

ACI committee documents are intended for the use of individuals who are competent to evaluate the significance and limitations of its content and recommendations and who will accept responsibility for the application of the material it contains. Individuals who use this publication in any way assume all risk and accept total responsibility for the application and use of this information.

All information in this publication is provided “as is” without warranty of any kind, either express or implied, including but not limited to, the implied warranties of merchantability, fitness for a particular purpose or non-infringement.

ACI and its members disclaim liability for damages of any kind, including any special, indirect, incidental, or consequential damages, including without limitation, lost revenues or lost profits, which may result from the use of this publication.

It is the responsibility of the user of this document to establish health and safety practices appropriate to the specific circumstances involved with its use. ACI does not make any representations with regard to health and safety issues and the use of this document. The user must determine the applicability of all regulatory limitations before applying the document and must comply with all applicable laws and regulations, including but not limited to, United States Occupational Safety and Health Administration (OSHA) health and safety standards.

Participation by governmental representatives in the work of the American Concrete Institute and in the development of Institute standards does not constitute governmental endorsement of ACI or the standards that it develops.

Order information: ACI documents are available in print, by download, through electronic subscription, or reprint and may be obtained by contacting ACI.

Most ACI standards and committee reports are gathered together in the annually revised the ACI Collection of Concrete Codes, Specifications, and Practices.

American Concrete Institute
38800 Country Club Drive
Farmington Hills, MI 48331
Phone: +1.248.848.3700
Fax: +1.248.848.3701

www.concrete.org

ACI PRC-237.2-21

Form Pressure Exerted by Self-Consolidating Concrete: Primary Factors and Prediction Models—Report

Reported by ACI Committee 237

Anton K. Schindler*, Chair

Lloyd J. Keller*, Secretary

Mohamed Bassuoni
Claude Bedard
Peter H. Billberg
Joseph A. Daczko
Geert De Schutter
Kirk K. Deadrick
Liberato Ferrara
Dimitri Feys
G. Terry Harris
Jiong Hu
Venkatesh S. Iyer
Samuel Keske
Kamal H. Khayat*‡
Eric P. Koehler
David A. Lange*
Darmawan Ludirdja
George Morcous
H. Celik Ozyildirim
Eric S. Peterson*
Ketan R. Sompura
Mohammed Sonebi
Caroline M. Talbot
Nathan A. Tregger
Stacia Van Zetten*
Olafur H. Wallevik
Kejin Wang
Ammar Yahia

Consulting Members

Erika E. Holt
Gary F. Knight
Caijun Shi

*Voting members who led the development of this report.
‡Subcommittee Chair.

The committee acknowledges K. Vallurupalli, A. Omran, M. Matias, L. Proietti, and D. Toon for their contributions to this report.

Given the high flowability and relatively fast casting rate of self-consolidating concrete (SCC), such concrete can exert high form pressure. Accurate assessment of form pressure is necessary from safety and economic points of view. The maximum form pressure and pressure decay are dependent on the structural buildup of the concrete at rest following placement, as well as on the placement parameters. The structural buildup at rest is affected by the thixotropy of the mixture. This report presents information on key parameters, including constituent materials; mixture proportioning; and casting parameters such as the casting rate, concrete temperature, and reinforcement percentage, affecting thixotropy and SCC form pressure. Prediction models available for estimating SCC form pressure are presented. Findings from two round-robin field studies conducted to validate these models are also discussed. This report should be of interest to concrete professionals, including concrete suppliers and formwork designers, because it covers: 1) the influence of SCC proportions and casting parameters on form pressure; 2) means to estimate formwork pressure with examples; and 3) techniques to measure formwork pressure in field applications.

Keywords: form pressure; lateral pressure; self-consolidating concrete; structural buildup at rest; thixotropy.

CONTENTS

ACI PRC-237.2-21 was adopted and published July 2021.

CHAPTER 1—INTRODUCTION

1.1—Introduction

Self-consolidating concrete (SCC) is highly flowable non-segregating concrete that can spread into place, fill the formwork, and encapsulate the reinforcement without any mechanical consolidation. SCC is designed to have a relatively low yield stress compared to conventional concrete to ensure high flowability without segregation. Yield stress corresponds to the critical shear stress value beyond which the material starts to flow. SCC can have slump flow values typically in the range of 22 to 30 in. (560 to 760 mm). Due to the high fluidity of SCC, formwork systems are often designed to sustain full hydrostatic pressure. Accurate estimation of form pressure for field application of SCC is necessary for the economical design of formwork and to ensure safety during and after casting. Field and laboratory investigations involving the measurement of lateral pressure exerted by SCC on formwork systems indicate that form pressure can be considerably lower than hydrostatic pressure (Assaad and Khayat 2005c; Assaad et al. 2003b; Billberg et al. 2014; Gardner et al. 2016). This is illustrated in Fig. 1.1 for SCC used for the rehabilitation of wall elements that measure 20 ft (6 m) in height, 23 ft (7 m) in length, and 7.5 in. (0.19 m) in width (Assaad 2004; Khayat et al. 2005b). The casting rate was approximately 21 ft/h (6.5 m/h). The pressure distribution envelopes exerted by a representative SCC mixture determined at the end of the placement and then after 1 and 3 hours are shown in Fig. 1.1 (left). The variations in the maximum lateral pressure with time for five different SCC mixtures that were proportioned with different thixotropic values are illustrated in Fig. 1.1 (right).

Form pressure is affected by structural buildup; structural buildup increases with rest time, hence reducing form pressure (Assaad et al. 2003b; Assaad and Khayat 2005c). The rate of structural buildup is dependent on the concrete mixture characteristics, including:

(a) Binder constituent (Assaad et al. 2003b)
(b) Type and dosage of chemical admixtures (Assaad et al. 2003b; Khayat and Assaad 2006)
(c) Water-cementitious materials ratio (*w*/*cm*) (Khayat and Assaad 2006)
(d) Maximum aggregate size and the total aggregate content (Assaad and Khayat 2005a)

For a given casting rate R, lower form pressure can be observed for concrete with a higher rate of structural buildup at rest (Assaad and Khayat 2007). The structural buildup of the concrete corresponds to an increase in shear strength when the material is left at rest due to flocculation—a physical effect that is reversible—as well as hydration of the cement-based materials, which is irreversible. At very early age, the flocculation component is dominant, and the structural buildup is reversible and can be broken down if the mixture is agitated. However, as hydration progresses with time, the structural buildup gradually becomes less reversible (Roussel et al. 2012). The placement of SCC mixtures with a high rate of structural buildup, at relatively low to moderate casting rates—for example, approximately 7 to

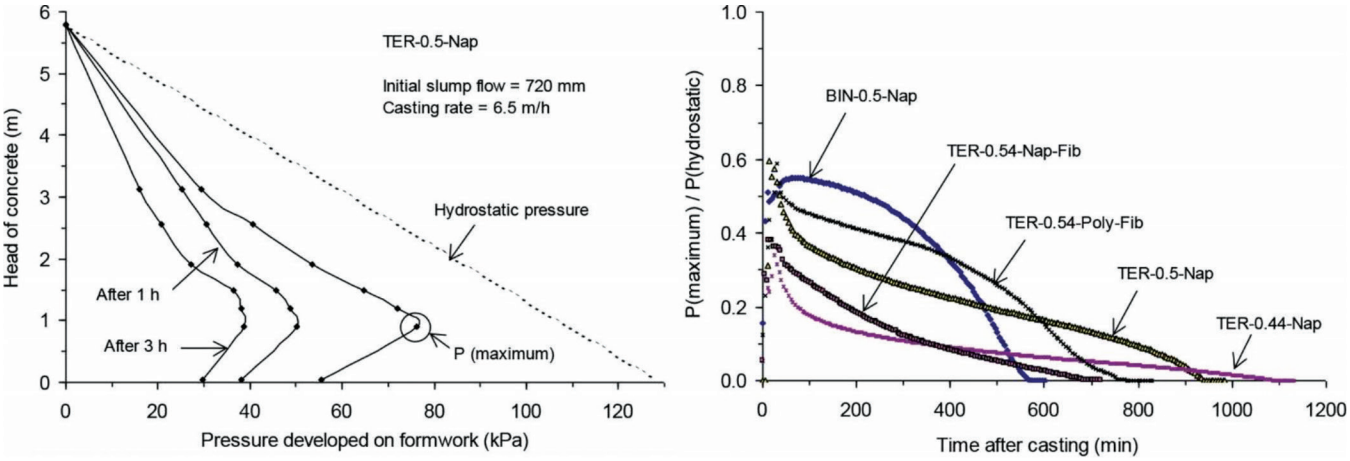

Fig. 1.1—Variations of lateral pressure with height (left) and P(maximum)/P(hydrostatic) *values for the five tested SCC mixtures (right) (Assaad 2004; Khayat et al. 2005b). (Note: 1 m = 3.3 ft; 1 kPa = 0.145 psi.)*

16 ft/h (2 to 5 m/h)—can result in lateral pressures on the order of 50 to 60% of hydrostatic pressure (Khayat and Omran 2010b; Omran et al. 2014).

In addition to SCC mixture characteristics, form pressure is affected by the casting parameters, including:

(a) Casting rate (Assaad and Khayat 2007)
(b) Concrete temperature (Omran et al. 2014)
(c) Waiting period between successive lifts (Omran et al. 2014)
(d) Formwork material (Arslan et al. 2005; Omran and Khayat 2017a)
(e) Minimum formwork dimension (Omran and Khayat 2017a)
(f) Reinforcement percentage (Perrot et al. 2009).

The casting rate for SCC can vary by construction type (new construction or repair) and size of the member. Concrete temperature, casting rate, and waiting period between the successive lifts influence the structural buildup of SCC, thereby affecting the form pressure (Omran et al. 2014). Formwork materials and their dimensions (Omran and Khayat 2017a), reinforcement percentage (Omran and Khayat 2017b; Perrot et al. 2009), and the density (unit weight) of the SCC contribute to the net weight supported by the formwork and the resulting formwork pressure. Additionally, the form pressure is also affected by various other factors, such as the placement method used (pumping or chute) (Assaad and Khayat 2007), formwork leaks, tie placement, and nearby vibration (heavy traffic). As a result, jobsite controls or form-monitoring strategies (ACI SP-4 [2014] Chapters 11 and 12; ACI 347R-14 Chapter 5) should be employed by the contractor before, during, and after casting. Various theoretical and empirical models have been developed for the assessment of form pressure exerted by SCC, and some of the most prevalent models will be covered in this report.

1.2—Scope

The objective of this report is to provide detailed information to concrete professionals, including concrete suppliers and formwork contractors, with respect to the main SCC mixture characteristics and casting parameters that influence form pressure. This report also presents the most prevalent models to estimate form pressure available to assess form pressure exerted by SCC, and the accuracy of these models are evaluated based on measurements collected from two round-robin field studies.

The development of factors of safety for use in formwork design, including those used for allowable stress design (ASD) and load and resistance factor design (LRFD) methodologies, is outside the scope of this report. The correction factors or safety factors will be dependent upon the capability of the ready mixed concrete producer to control the rheological parameters of the SCC mixture.

Additionally, test procedures for measuring thixotropy and other parameters needed for determining form pressure using these models are discussed. Details regarding the instrumentation needed for field measurement of form pressure and major round-robin field studies conducted to validate these models are presented.

Chapter 2 presents notation and definitions specific to this document. Chapter 3 describes the thixotropy of cement-based materials, test methods, and the effect of thixotropy on SCC form pressure. Chapters 4 and 5 identify the main material and casting parameters that influence form pressure characteristics, respectively. Chapter 6 presents the primary models available to estimate SCC form pressure. Chapter 7 discusses the results of two major round-robin field validation studies conducted in 2012 and 2014 to evaluate the suitability of various models to estimate SCC form pressure. Chapter 8 summarizes the key findings from this report.

1.3—Use of U.S. Customary Units in this report

In this document and in accordance with standard ACI and U.S. construction industry practice, lb is used as the unit abbreviation for either mass or force, as is evident in, for example, ACI 318-19 and ACI 347R-14. Two examples from ACI 318-19 are provided to help clarify this practice:

(1) Mass: w_c = density of concrete, lb/ft^3
(2) Force: T_t = total test load, lb

CHAPTER 2—NOTATION AND DEFINITIONS

2.1—Notation

$IP\tau_{0rest}$ = yield stress at rest measured using inclined plane test setup, psi (Pa)

$IP\tau_{0rest}(t)$ = rate of gain in yield stress with time of rest measured using inclined plane test setup, psi/min (Pa/min)

$P_{hydrostatic}$ = equivalent hydrostatic pressure, psi (Pa)

P_{max} = maximum lateral pressure exerted by concrete on formwork, psi (Pa)

$PV\tau_{0rest}$ = yield stress at rest measured using portable vane test setup, psi (Pa)

$PV\tau_{0rest}(t)$ = rate of gain in yield stress with time of rest measured using portable vane test setup, psi/min (Pa/min)

R = casting rate, ft/h (m/h)

τ_{0rest} = yield stress at rest, psi (Pa)

$\tau_{0rest}(t)$ = rate of gain in yield stress with time of rest; also referred to as A_{thix}, psi/min (Pa/min)

w_c = density (unit weight) of concrete, lb/ft^3 (kg/m^3)

w/c = water-cement ratio, by mass

w/cm = water-cementitious materials ratio, by mass

w/p = water-powder ratio, by mass; w/p is only used in mixtures containing a filler as a partial replacement of portland cement, such as limestone filler

2.2—Definitions

Please refer to the latest version of ACI Concrete Terminology for a comprehensive list of definitions. Definitions provided herein complement that resource.

casting rate—vertical rate of concrete deposition into the formwork.

cohesion—ability of concrete to hold together due to the flocculation and hydration of the particles.

filling ability (unconfined flowability)—ability of SCC to flow into and fill completely all spaces within the formwork, under its own weight.

flocculation—clustering of binder particles in cement paste at rest caused by interparticle forces, in part responsible for thixotropy, which results in an increase in yield stress.

lateral pressure cancelation—time corresponding to the time elapsed when the measured lateral pressure reaches zero.

passing ability (confined flowability)—ease with which concrete can pass among various obstacles and narrow spacing in the formwork without blockage.

pressure decay—decrease in the lateral pressure exerted by the concrete on the formwork with an increase in resting time.

rheology—science of deformation and flow of matter; evaluated using rheometers that enable one to relate variations in shear stress to shear rate.

shear thinning—decrease in viscosity with increasing shear rate during steady shear flow.

slump flow—measure of unconfined flow potential of a freshly mixed self-consolidating concrete; value is equal to the average of two perpendicular diameters of the material measured to the nearest 1/2 in. (10 mm) after it is released from the slump cone and stops flowing.

stability—ability of a material to maintain the homogeneous distribution of its various constituents during its flow and setting.

structural breakdown—decrease in the viscosity when a constant shear rate is applied to the material at rest; decrease is due to the breakage of the flocculated particles and hydration products.

structural buildup—increase in shear stress when the material is left at rest due to flocculation and hydration.

yield stress—critical shear stress value below which an ideal plastic or viscoplastic material behaves like a solid (that is, will not flow); once the yield stress is exceeded, a plastic material yields (deforms plastically), while a viscoplastic material flows like a liquid.

yield stress at rest—represents static yield stress of the material—that is, minimum shear stress needed to initiate flow measured after a given time of rest.

CHAPTER 3—THIXOTROPY AND FORM PRESSURE

Understanding thixotropy is critical to the understanding of self-consolidating concrete (SCC) form pressure, and subsequent chapters of this report cite the effects of concrete materials and mixture proportioning as well as placement conditions (for example, temperature) on SCC thixotropy and form pressure. This chapter discusses the principles of thixotropy, methods available to measure it, and the relationship between thixotropy and form pressure. Refer to ACI 238.2T for further information on thixotropy.

3.1—Thixotropy

According to ACI 238.2T, thixotropy is a reversible, isothermal, time-dependent decrease in viscosity when a fluid is subjected to an increase in shear stress or shear rate; therefore, when the fluid is at rest, viscosity increases back to its original value. Thus, thixotropy can be considered as the continuous decrease of viscosity with time when there is an increase in shear stress or shear rate causing flow to occur, and the subsequent recovery of viscosity in time when the shearing is discontinued (Mewis 1979; Mewis and Wagner 2009). Thixotropy should be distinguished from irreversible changes in viscosity. Such changes may be caused by hydration of the cementitious materials. Form pressure developed by SCC is a function of both the reversible structural changes due to thixotropy and the irreversible structural changes due to hydration (Assaad and Khayat 2005c; Assaad et al. 2003b).

Thixotropy of cement-based materials is strongly dependent on the mixture characteristics, mixing, and casting parameters such as casting rate. Tattersall and Banfill (1983) reported that cement characteristics such as packing density, fineness, and chemical composition can significantly affect thixotropy. When a cement-based suspension is sheared, its network structure is broken and, with continued shearing, there is eventually an equilibrium state at which no addi-

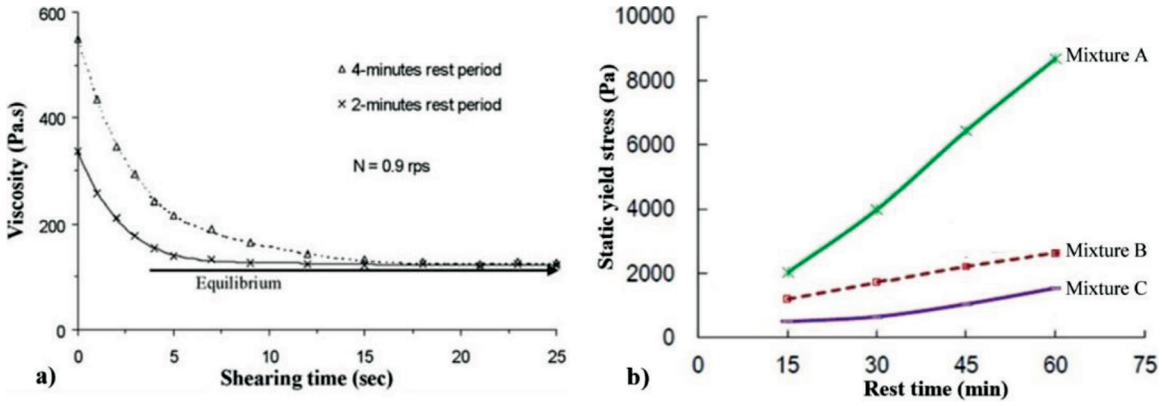

Fig. 3.1—Thixotropy in terms of: (a) structural breakdown measured as variation of viscosity with time for concrete after 2 and 4 minutes of rest (Assaad et al. 2003a); and (b) structural buildup for concretes with different degrees of thixotropy measured as variation of static yield stress with rest time (Omran et al. 2011). (Note: 1 Pa = 0.000145 psi.)

tional deflocculation happens in the paste. When shearing is stopped—that is, the suspension is at rest—the particles undergo reflocculation to form a network structure.

The influence of rest time on thixotropy is shown in terms of the structural breakdown in Fig. 3.1(a) (Assaad et al. 2003a) and structural buildup in Fig. 3.1(b) (Omran et al. 2011). In Fig. 3.1(a), the concrete is subjected to a constant rotational velocity of 0.9 revolutions per second (rps) after leaving it to rest for 2 minutes. The application of the rotational velocity resulted in breakdown of the flocculated structure. Such breakdown with time indicates that the concrete is thixotropic. An equilibrium structure is achieved after approximately 10 seconds in Fig. 3.1(a), where a balance between flocculation and deflocculation is reached. When shearing is stopped, and the material is allowed to rest for 4 minutes, the material is then resheared at the same rotational velocity of 0.9 rps. The results in Fig. 3.1(a) show that the measured viscosity is initially higher, indicating reflocculation during the rest time, and eventually a decrease in the viscosity to the same equilibrium value, indicating the reversible behavior of thixotropy. During the rest time, the reflocculation of individual particles happens. In addition to the flocculation, hydration products can also form between particles, leading to a further increase in structural buildup (Khayat et al. 2002; Roussel et al. 2012). The longer the material is at rest, the more the structural buildup becomes significant, thus requiring higher stress to break down the structure. This increase in the structural buildup is measured in terms of the change in static yield stress with rest time in Fig. 3.1(b). The three mixtures shown in Fig. 3.1(b) exhibit different levels of thixotropic behavior in that all show an increase in static yield stress with time. SCC Mixture A has a higher thixotropy than Mixtures B and C, as it exhibits greater static yield stress values after rest periods of 15 to 60 minutes. The rheology test protocol for the determination of the static yield stress is presented in Section 3.2.

3.2—Thixotropy test methods

There are numerous test methods that can be used to quantify the thixotropy and structural buildup of concrete. These experiments often consist of either conducting rheological tests at a constant shear rate, such as steady-state flow curves (Ghezal et al. 2002; Tattersall and Banfill 1983) and stress-growth tests (Assaad et al. 2003a), or using varied sheared rates such as hysteresis curves (Ish-Shalom and Greenberg 1960; Wallevik 2003) and breakdown area curves (Khayat et al. 2002). Steady-state flow, hysteresis, and breakdown area curves measure thixotropy in terms of the breakdown of the structure, whereas stress growth tests measure the structural buildup. The breakdown of the structure quantifies the reversible structural changes due to thixotropy, whereas the structural buildup measurements include both reversible structural changes due to thixotropy and the irreversible structural changes due to hydration. In this Report, emphasis is placed on structural buildup measurements as the form pressure estimation models (Khayat and Omran's [2010b] and Ovarlez and Roussel's [2007] models) described in Chapter 6 include the structural buildup as a parameter.

3.2.1 *Structural buildup measurement*—One of the ways of quantifying structural buildup is to measure the yield stress of the material at rest (τ_{0rest}). τ_{0rest} indicates the strength and number of interparticle bonds that are ruptured due to the applied shear or stress (Tattersall and Banfill 1983). The rheology test protocol for the determination of τ_{0rest} (also referred to as static yield stress and shear-growth yield stress) consists of applying a small rotational velocity (that is, 0.03 rps) to a vane immersed into fresh concrete (or mortar) and recording the variations of torque as a function of time, as shown in Fig. 3.2.1a. The shear-growth profile in Fig. 3.2.1a shows a linear-elastic region followed by a yielding moment where the torque exerted on the vane shaft reaches a maximum value corresponding to the beginning of flow. The maximum value during this profile corresponds to τ_{0rest}. The presence of such maximum torque response can be explained by the concept of structural deformation and breakdown of the bond in the flocculated system (Barnes 1997; Dzuy and Boger 1985). The calculation of τ_{0rest} from the measured maximum torque (T_{max}) requires knowledge of the geometry of the yield surface and shear stress distribution on the surface. Dzuy and Boger (1985) assumed that

the material is sheared along a localized cylindrical surface circumscribed by the vane, and this shear stress is uniformly distributed over this surface. Based on this assumption, a good approximation of τ_{0rest} can be calculated as per Eq. (3.2.1a). The details regarding the derivation and assumptions used for estimation can be found in Koehler and Fowler (2004).

$$\tau_{0rest} = \frac{T_{max}}{K} \quad (3.2.1a)$$

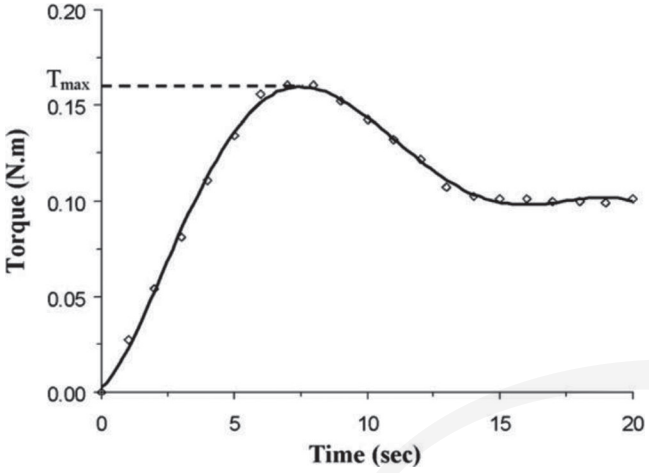

Fig. 3.2.1a—Typical torque-time profile for SCC with 26 in. (650 mm) slump flow at a constant rotational velocity of 0.03 rps (Assaad et al. 2003a). (Note: 1 N·m = 0.735 lb-ft.)

$$K = 2\pi r^2 H + \frac{4}{3}\pi r^3$$

where K is a constant and H and r are the height and radius of the vane.

The change in concrete yield stress with resting time can also be used to determine the degree of structural buildup and is expressed as the rate of gain in yield stress with the time of rest ($\tau_{0rest}(t)$). The portable vane test is a simplified and manual version of the aforementioned test and consists of determining the minimum torque needed to shear the mortar or concrete after a certain period of rest. A torque wrench is attached to the vane shaft and twisted to shear the tested materials at a constant speed of 10 to 15 seconds per quarter turn at the specified rest times. The peak torque value (T_{max}; Fig. 3.2.1a) needed to break down the inter-structural bonds and, thus, overcoming the yield stress of the material is noted. The sheared surface corresponds to a cylindrical surface of the interface between the outer diameter of the vane and sheared test sample. To prevent the entire sample from rotating in case of a plug flow of the test sample, a square container is used for the sample holder (Omran et al. 2011). The portable vane shown in Fig. 3.2.1b has four vanes of different sizes to determine yield stress at different times of rest. The variations of yield stress at rest measured using the portable vane ($PV\tau_{0rest}$) for SCC mixtures with slump flow values between 24 and 28 in. (600 and 720 mm) were determined using four vanes of different sizes (Fig. 3.2.1b). The results in Fig. 3.2.1c show that the $PV\tau_{0rest}$ increased

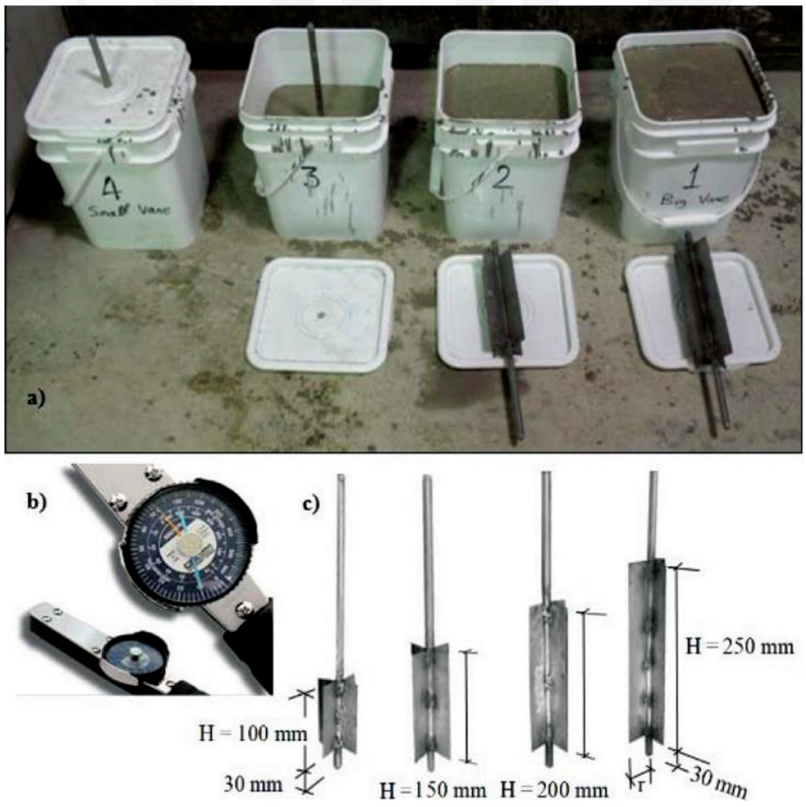

Fig. 3.2.1b—Portable vane test setup: (a) square containers; (b) torque meter; and (c) vanes of different sizes (Omran et al. 2011). (Note: 1 mm = 0.394 in.)

in a linear fashion over 60 minutes of rest. Thixotropy can be quantified as the slope of each line ($\tau_{0rest}(t)$), as well as the multiplication of τ_{0rest} and $\tau_{0rest}(t)$. A single size of vane can also be used with a sample of different heights; refer to portable vane test (Omran et al. 2011) for further information about the portable vane test method.

For the purpose of form pressure prediction, it is recommended that the measurement of thixotropy is done as soon as practical after the completion of mixing and agitation. It is recommended to perform at least three static yield tests to determine thixotropy by using 30- to 60-minute rest times to ensure that the rate of increase in static yield stress is linear, as indicated in Fig. 3.2.1c.

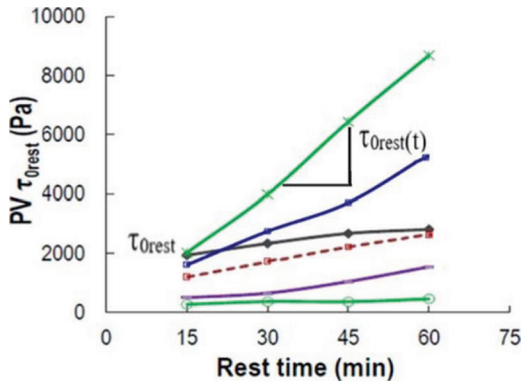

Fig. 3.2.1c—Typical variations of yield stress as a function of rest time for SCC mixtures determined using portable vane test (Omran et al. 2011). (Note: 1 Pa = 0.000145 psi.)

As an alternative to a rheometer, Khayat et al. (2010) developed an inclined plane test setup for measuring τ_{0rest} and $\tau_{0rest}(t)$. The inclined plane test setup consists of a movable plate whose inclination (θ) can be adjusted as shown in Fig. 3.2.1d. To measure τ_{0rest} for mortar or SCC, the sample is placed on the movable plate and is slowly lifted. Details regarding the volume and placement of the sample can be found in Khayat et al. (2010).

Depending on the value of θ, the gravitational (F_g) and frictional (F_k) forces acting on the sample along the inclined plane vary as shown in Fig. 3.2.1e. In the case of a solid sample, at a critical value of θ, the sample would begin to slide downward, and this sliding initiates when F_g is equal to F_k. However, for fresh mortar or SCC samples, if F_k is high enough to prevent sliding of the entire sample (achieved by increasing the roughness of the surface by covering it with sandpaper), shearing of the top layer occurs, resulting in the flow of the material, as shown in Fig. 3.2.1e(b). The critical angle (α) at which shearing happens and the vertical height to which the plate is lifted is used for estimation of τ_{0rest}, as shown in Eq. (3.2.1b). The test is conducted on samples

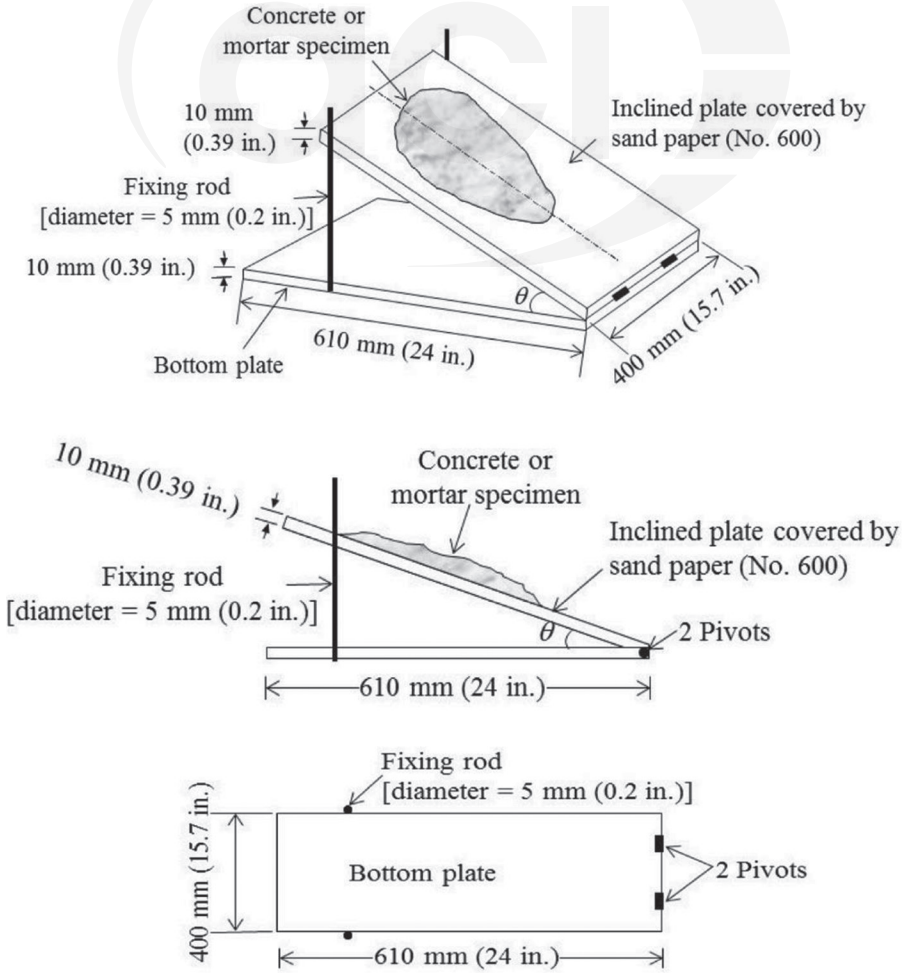

Fig. 3.2.1d—Schematic of the inclined plane test (Khayat et al. 2010).

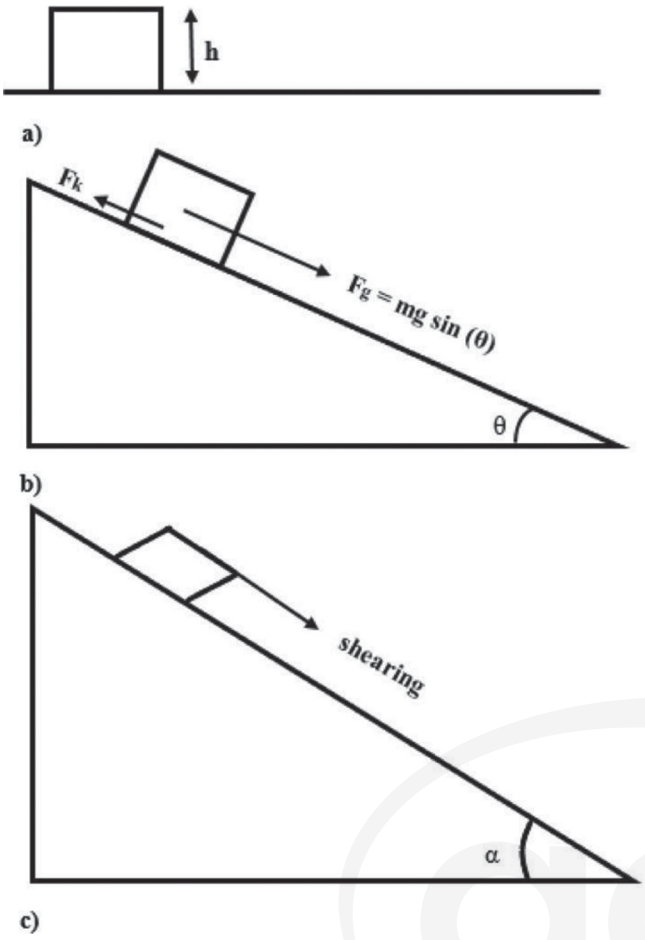

Fig. 3.2.1e—(a) SCC sample at zero inclination; (b) forces acting along the inclined plane on mass m *at inclination angle θ; and (c) shearing of the sample indicating flow initiation at critical angle α (Khayat et al. 2010).*

subjected to different rest times to measure $\tau_{0rest}(t)$ and results of yield stress at rest obtained using the inclined plane test for SCC mixtures with different mixture compositions and slump flow values ranging between 22 and 28 in. (560 and 720 mm) are shown in Fig. 3.2.1f.

$$IP\tau_{0rest} = \rho g h \sin\alpha \qquad (3.2.1b)$$

where h is the thickness of the spread of SCC at the horizontal position; ρ is SCC density; α is the critical angle at which shearing of the sample occurs; and g is the acceleration due to gravity.

Amziane et al. (2008) developed an alternative approach known as the plate test for measuring τ_{0rest} and $\tau_{0rest}(t)$ for thixotropic materials. The schematic of the plate test setup is shown in Fig. 3.2.1g. The test setup consists of a plate attached below a balance and is partly immersed in SCC. The plate is covered with sandpaper with an average roughness of 0.008 in. (200 μm) to prevent slippage between the plate and the SCC; this roughness corresponds to a grit size of 70 or a U.S. mesh of 60. The apparent mass of the plate is monitored over time. The plate remains static during the test, and the change in apparent mass is attributed to mobilization

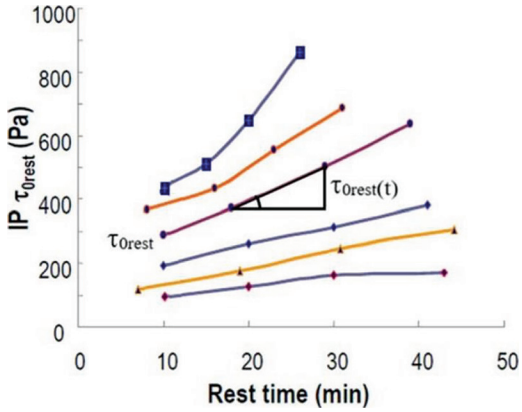

Fig. 3.2.1f—Yield stress variation with rest time for SCC mixtures measured using inclined plane test; SCC had different mixture compositions and slump flow values of 22 to 28 in. (560 to 720 mm) (Khayat et al. 2010). (Note: 1 Pa = 0.000145 psi.)

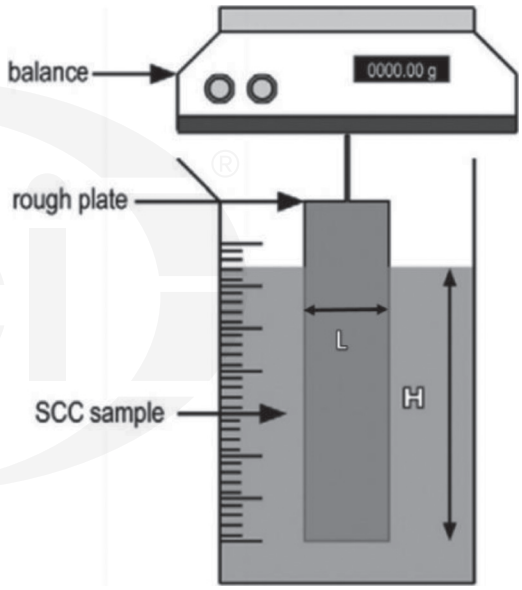

Fig. 3.2.1g—Schematic of plate test setup (Perrot et al. 2009).

of shear stress on the plate due to the slight deformation in the test material (mortar or concrete) under its own weight, which includes deformation due to settlement, segregation, bleeding, and evaporation of the test material. This deformation is limited at early age but sufficient to reach a critical value inducing material yielding. As a result, the mobilized shear stress can be considered τ_{0rest}. The dimensions of the plate are 0.1 in. (3 mm) thick, 3 in. (75 mm) wide and 4 in. (100 mm) long, and the concrete is placed to a height of 8 in. (200 mm) in a vessel made of smooth polyvinyl chloride (PVC) and has dimensions of 8 in. (200 mm) diameter and 8 in. (200 mm) in height. These dimensions are chosen such that the vessel is large enough compared to the size of the plate so that material can be assumed to be homogenous. To avoid losses due to evaporation and its influence on the apparent mass measured, an oil film is added on the top of

the material. $\tau_{0rest}(t)$ is calculated from apparent mass evolution ($\Delta M(t)$) using Eq. (3.2.1c).

$$\tau_{0rest}(t) = \frac{g\Delta M(t)}{2S} \quad (3.2.1c)$$

where S is the area of the immersed surface—that is, plate width (L) times the immersed height (H).

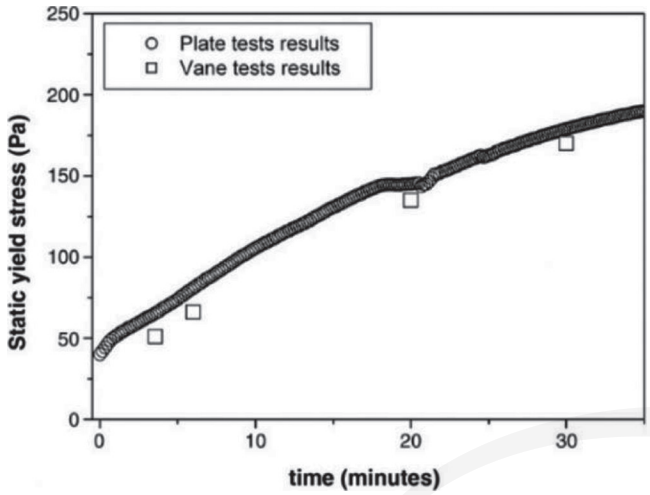

Fig. 3.2.1h—Comparison between calculated static yield stress values of SCC using the plate test and measured static yield stress values using a vane rheometer (Perrot et al. 2009). (Note: 1 Pa = 0.000145 psi.)

The comparison between the calculated yield stress values using the plate test and measured yield stress values using a vane rheometer for SCC with a water-cement ratio (w/c) of 0.47 is shown in Fig. 3.2.1h.

3.3—Influence of thixotropy on form pressure

Concrete that can exhibit a higher degree of thixotropy (that is, a higher rate of structural buildup) can develop greater cohesiveness soon after casting, thus acting as a cohesive body exerting less pressure than the full-hydrostatic pressure state. Khayat and Omran (2010b) evaluated the relationship between the form pressure characteristics and the structural buildup of SCC mixtures. The lateral pressure values were measured at different depths in the formwork—that is, 3.3, 13.1, 26.2, and 39.4 ft (1, 4, 8, and 12 m)—and the structural buildup of the mixtures were assessed by measuring τ_{0rest} after 15 minutes of rest ($\tau_{0rest@15min}$) and $\tau_{0rest}(t)$ using the portable vane test setup. Based on the results, a linear relationship (R^2 ranging from 0.82 to 0.92) was observed between the lateral pressure and structural buildup measured using different indexes—that is, $\tau_{0rest@15min}$, $\tau_{0rest}(t)$, $\tau_{0rest@15min} \times \tau_{0rest}(t)$ as shown in Fig. 3.3a, 3.3b, and 3.3c, respectively. Additionally, the lateral pressure decay during the first 60 minutes after casting and the pressure decay until reaching the pressure cancellation time (t_c) were correlated with the structural buildup as shown in Fig. 3.3d, 3.3e, and 3.3f.

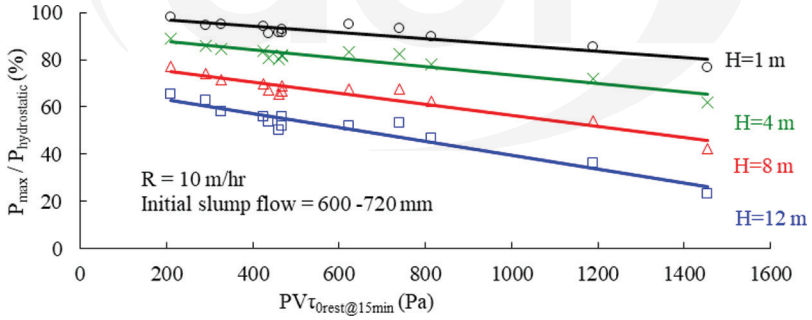

Fig. 3.3a—Variations of relative lateral pressure with $PV\tau_{0rest@15min}$ at different heights of placement (adapted from Khayat and Omran [2010b]). (Note: 1 m = 3.3 ft; 1 mm = 0.0394 in.; 1 Pa = 0.000145 psi.)

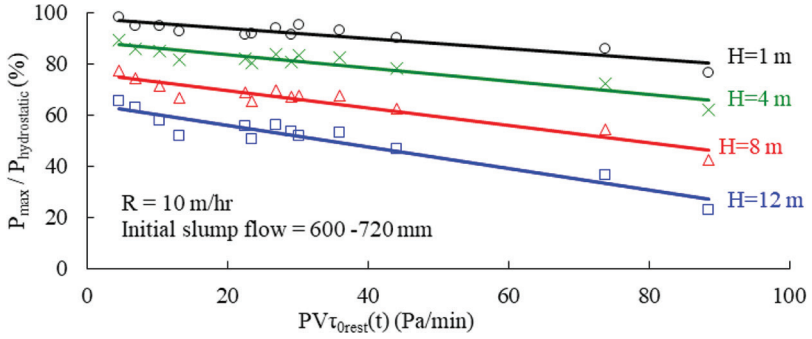

Fig. 3.3b—Variations of relative lateral pressure with $PV\tau_{0rest}$(t) at different heights of placement (adapted from Khayat and Omran [2010b]). (Note: 1 m = 3.3 ft; 1 mm = 0.0394 in.; 1 Pa = 0.000145 psi.)

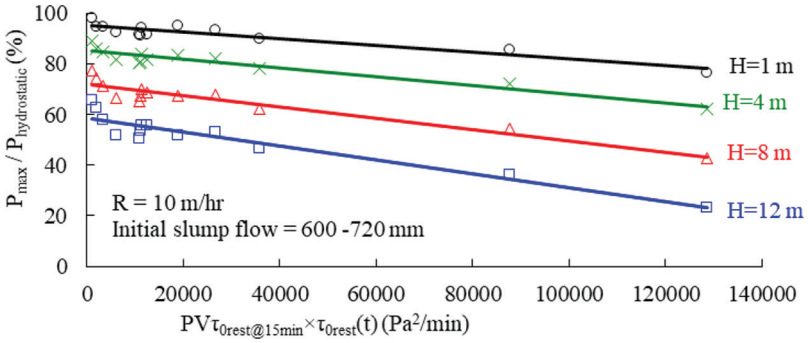

Fig. 3.3c—Variations of relative lateral pressure with $PV\tau_{0rest@15min} \times \tau_{0rest}(t)$ *at different heights of placement (adapted from Khayat and Omran [2010b]). (Note: 1 m = 3.3 ft; 1 mm = 0.0394 in.; 1 Pa = 0.000145 psi.)*

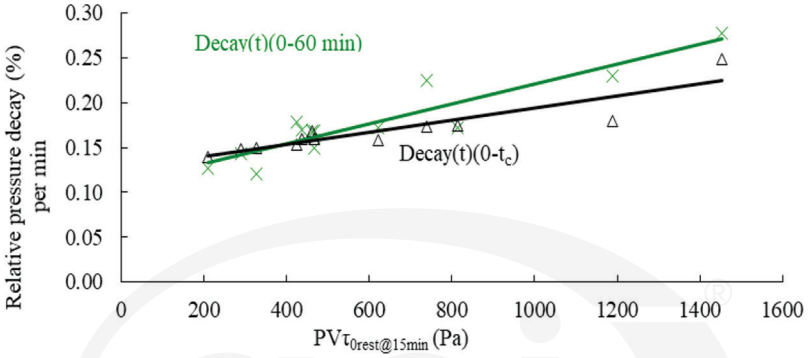

Fig. 3.3d—Variations of relative pressure decay with $PV\tau_{0rest@15min}$ *(Khayat and Omran 2010b). (Note: 1 Pa = 0.000145 psi.)*

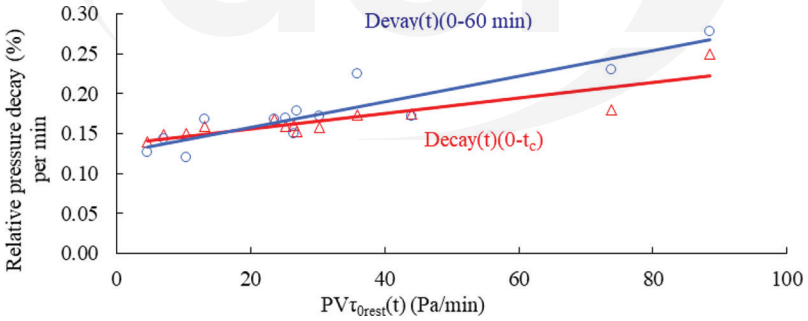

Fig. 3.3e—Variations of relative pressure decay with $PV\tau_{0rest}(t)$ *(Khayat and Omran 2010b). (Note: 1 Pa = 0.000145 psi.)*

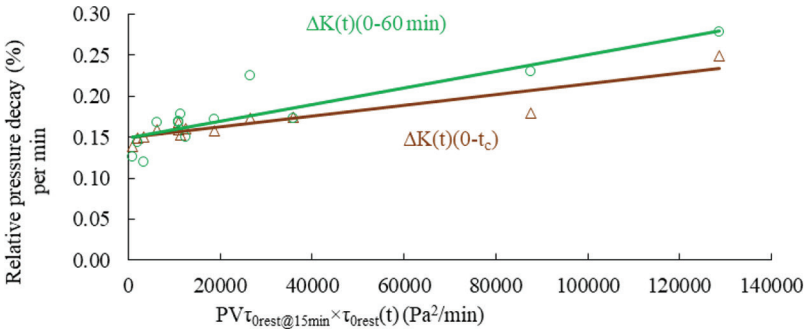

Fig. 3.3f—Relative pressure decay versus $PV\tau_{0rest@15min} \times \tau_{0rest}(t)$ *(Khayat and Omran 2010b). (Note: 1 Pa = 0.000145 psi.)*

Table 4.1—Overall effect of increasing mixture proportioning parameters on form pressure*

Increase of	Initial lateral pressure	Pressure decay	Main reason
Binder content (lowering *w/cm*; fixed HRWRA)	Decrease	Faster	Increase in thixotropy (Billberg 2006)
Aggregate content	Decrease	Faster	Increase in internal friction amplified by increased aggregate content decreases the mobility of concrete (Assaad and Khayat 2005a; Omran et al. 2012)
Maximum size of aggregate (MSA)	Decrease or limited effect	Faster or limited effect	Depends on variation in the packing density with changes in MSA (Assaad and Khayat 2005a)
Paste content (fixed *w/cm*)	Increase (1)	Faster (2)	(1) Decrease in internal friction due to lower coarse aggregate volume (2) Increase in cohesion due to higher paste content (Alexandridis and Gardner 1981; Assaad and Khayat 2004b; Omran et al. 2012)
Water content (reduced HRWRA to maintain fixed slump flow)	Increase (1)	Faster, slower, or no change (2)	(1) Low shear strength properties due to high water content (2) Depends on the workability retention characteristics of the HRWRA and the initial starting dosage being used. Some HRWRA's lose workability relatively quickly (less than 1 hour), while others are developed to maintain workability for longer times (greater than 2 hours) (Khayat and Assaad 2006).*†
HRWRA content† (fixed *w/cm*)	Increase	Faster, slower, or no change	Depends on the workability retention characteristics of the HRWRA and the initial starting dosage being used. Some HRWRAs lose workability relatively quickly (less than 1 hour), while others are developed to maintain workability for longer times (greater than 2 hours) (Khayat and Assaad 2006).*,†
VMA† (fixed initial slump flow and increased HRWRA dosage)	No change or increase (1)	Slower (2)	(1) Depending on VMA type and dosage, HRWRA demand can vary, leading to either no significant change in initial pressure or a slight increase in pressure at high VMA dosage (2) Higher HRWRA demand, especially if HRWRA improves slump retention (Assaad and Khayat 2006b; Khayat 1998)
VMA† (with fixed HRWRA—that is, reduced slump flow)	Decrease	Faster	Addition of VMA typically increases the degree of thixotropy (Prakash and Santhanam 2006; Ghio et al. 1994)
Set-retarding admixtures†	Increase/limited effect	Slower	Retards rate of cohesion development (Assaad et al. 2003b)
Set-accelerating admixtures†	Decrease/limited effect	Faster	Accelerates the rate of hydration (Assaad et al. 2003b)

*Observed behavior is based on studies listed in the references. General observations are valid for materials in use at specific ranges considered in these studies. Changing mixture proportioning parameters may affect other factors (for example, increasing VMA content normally increases HRWRA demand), which can affect form pressure characteristics.

†The reader should consult admixture manufacturers on the effect of chemical admixtures on form pressure characteristics. as the effect varies based on the chemical composition of the admixture and its interaction with other constituents including binders.

CHAPTER 4—EFFECT OF MIXTURE CHARACTERISTICS ON FORM PRESSURE

4.1—Introduction

The functional requirements in proportioning SCC include filling ability, passing ability, and stability. SCC proportioning is discussed extensively in ACI 237R. This section discusses how mixture proportioning for SCC has been found to affect form pressure characteristics.

Studies have shown that altering any of the following parameters that have a significant effect on thixotropy can affect lateral form pressure: cement type and content; supplementary cementitious material types and contents; *w/cm*; high-range water-reducing admixture (HRWRA) types and content; viscosity-modifying admixture (VMA) types and content; and aggregate size, gradation, and content. Table 4.1 summarizes the effect of these parameters on form pressure and pressure decay.

4.2—Binder constituents and content

Assaad and Khayat (2005b) investigated the effects of binder content and composition on form pressure using SCC. As illustrated in Fig. 4.2a, this study examined five different binder compositions, including mixtures made with

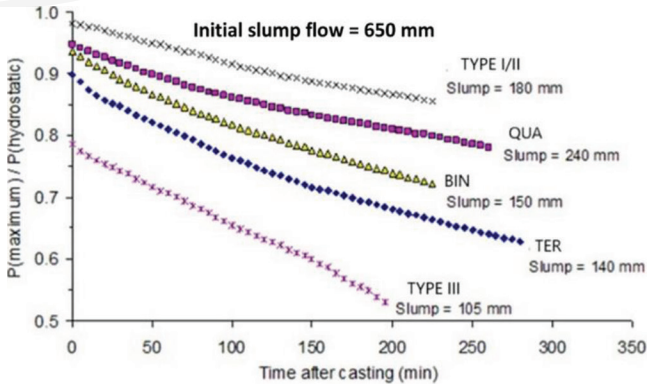

Fig. 4.2a—Variations in lateral pressure characteristics of SCC made with 450 kg/m³ (760 lb/yd³) of various binder types; slump values are those determined at the end of pressure monitoring. Slump values at end of pressure monitoring are noted (Assaad and Khayat 2005b). (Note: 1 mm = 0.394 in.)

Type I/II cement; Type III cement; binary binder (BIN) with silica fume (SF); a ternary binder (TER) with SF and Class F fly ash (FA); and a quaternary binder (QUA) with SF, FA, and slag (SL). The amounts of HRWRA and air-entraining admixture were adjusted to maintain constant initial slump

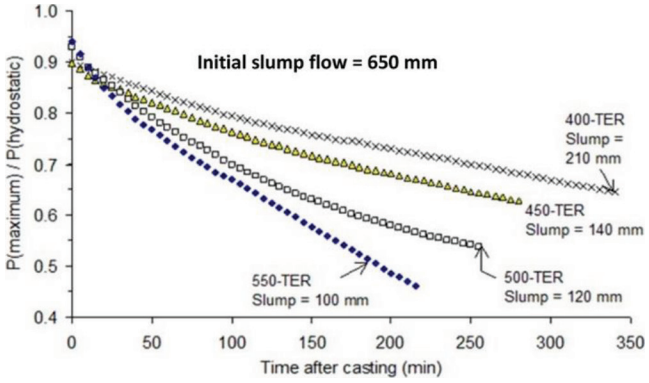

Fig. 4.2b—Variations in lateral pressure characteristics of SCC made with various contents of the ternary binder. Slump values at end of pressure monitoring are noted (Assaad and Khayat 2005b). (Note: 1 mm = 0.394 in.)

flow of 26 in. (650 mm). The VMA content was constant (4 oz. per 100 lb of cement [260 mL per 100 kg of cement]) in all mixtures.

For a given binder content, the binder composition significantly affected the initial lateral pressure and the pressure decay due to their varying degrees of thixotropy. The Type III cement had the lowest initial lateral pressure and the fastest pressure decay due to its high thixotropy. By comparing the ternary binder (6% SF, 22% FA, and 72% cement) content at values of 675, 760, 840, and 927 lb/yd^3 (400, 450, 500, and 550 kg/m^3), Assaad and Khayat (2005b) found increasing the binder content resulted in a slight increase in initial lateral pressure, as shown in Fig. 4.2b. Pressure decay depends significantly on the rate of structural buildup, thus the increase in binder content leads to sharper pressure decay. Similar results were observed by Omran et al. (2012) with increasing the binder content. The effect of supplementary cementitious materials (SCMs) and fillers depends on their physical and chemical properties (Andreas and Frank 2005; Assaad and Khayat 2005b).

4.3—Water content

Khayat and Assaad (2006) reported significant differences in lateral pressure and pressure decay with changes in *w/cm*. Keeping the slump flow consistent at 26 in. (650 mm), SCC with 760 lb/yd^3 (450 kg/m^3) binder (6% SF, 22% FA, and 72% cement) at *w/cm* 0.36, 0.40, and 0.46 were analyzed. Figure 4.3a (mixtures with carboxylate [PC]-based HRWRA) and Fig. 4.3b (mixtures with naphthalene [PNS]-based HRWRA) show that the mixtures with 0.46 *w/cm* exhibit greater initial pressure, as well as faster pressure decay compared to the other two mixtures. The high initial pressure at 0.46 *w/cm* was attributed to the increased water and paste contents as well as the reduction in coarse aggregate volume, leading to lower shear strength properties of the plastic concrete. The faster pressure decay was due to the reduction in HRWRA demand of the SCC made with 0.46 *w/cm*, which reduces the interference of the HRWRA on cement hydration.

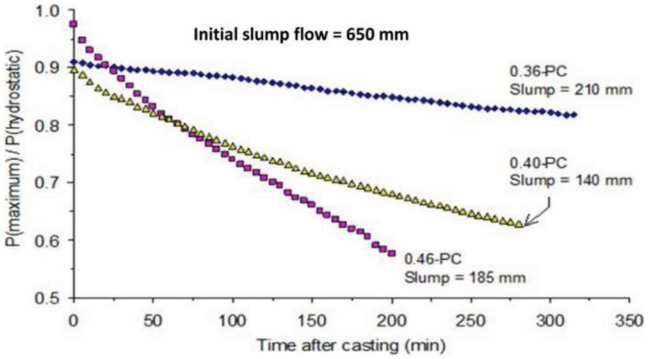

Fig. 4.3a—Effect of w/cm *on lateral pressure characteristics of SCC made with PC-based HRWRA. Slump values at end of pressure monitoring are noted (Khayat and Assaad 2006). (Note: 1 mm = 0.394 in.)*

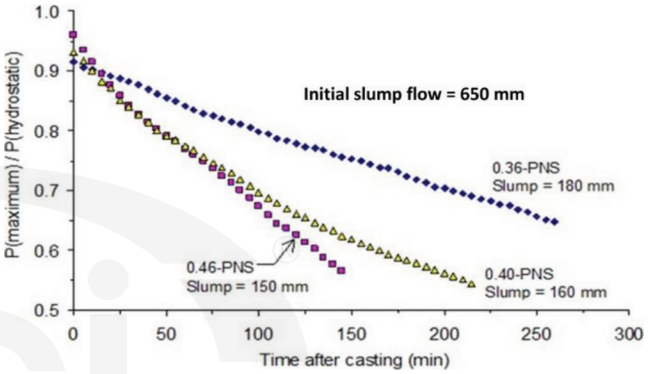

Fig. 4.3b—Effect of w/cm *on lateral pressure characteristics of SCC made with PNS-based HRWRA. Slump values at end of pressure monitoring are noted (Khayat and Assaad 2006). (Note: 1 mm = 0.394 in.)*

4.4—Aggregate characteristics

Aggregate properties, such as coarse aggregate content, gradation, the maximum size of aggregate (MSA), and packing density influence form pressure. Amziane and Baudeau (2000), using conventional concrete mixtures, showed that the maximum lateral pressure decreased as the volume of coarse aggregate increased. They suggested that the degree of internal friction is limited while the volume of mortar is dominant. Assaad and Khayat (2005a) found similar results for SCC mixtures with slump flow consistent at 26 in. (650 mm), ternary binder (6% SF, 22% FA, and 72% cement) at *w/cm* of 0.40. As illustrated in Fig. 4.4a, the decrease in the sand-to-total aggregate volume ratio from 1, 0.75, 0.50, 0.46, 0.40, 0.36, to 0.30, corresponding to coarse aggregate volumes of 0, 14.8, 29.9, 32.1, 35.8, 38.0, to 41.7%, respectively, resulted in a reduction of lateral pressure and an increase in pressure decay.

Amziane and Baudeau (2000) examined the effects of aggregate gradation and found higher lateral pressure when using discontinuously graded aggregate having a higher MSA compared to a continuously graded aggregate with a lower MSA. Assaad and Khayat (2005a) evaluated the effect of MSA—that is, No. 8, No. 7, and No. 67 (10, 14, and 20 mm) on lateral pressure characteristics of SCC mixtures with slump flow consistent at 26 in. (650 mm), ternary binder (6%

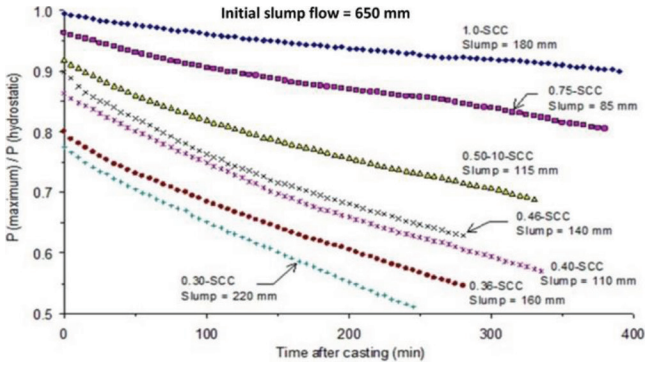

Fig. 4.4a—Variations of lateral pressure with time for mixtures made with different sand-to-total aggregate ratio of 0.30 to 1.0, which correspond to coarse aggregate contents of 0 to 41.7%, respectively. Slump values at end of testing are noted. (Assaad and Khayat 2005a). (Note: 1 mm = 0.394 in.)

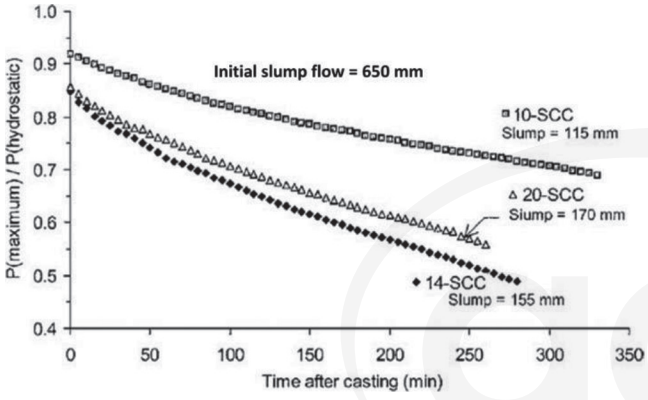

Fig. 4.4b—Variations of lateral pressure characteristics with time for mixtures made with different MSA. Slump values at end of testing are noted (Assaad and Khayat 2005a). (Note: 1 mm = 0.394 in.)

SF, 22% FA, and 72% cement) at *w*/*cm* of 0.40. As illustrated in Fig. 4.4b, the increase in the MSA from No. 8 to No. 7 (10 to 14 mm) resulted in the reduction of lateral pressure and increase in pressure decay. However, no significant change in the initial lateral pressure and slightly slower pressure decay was observed with the increase in the MSA from No. 7 to No. 67 (14 to 20 mm). This was attributed to the increase in the packing density from 56 to 62% with the increase in the MSA from No. 8 to No. 7 (10 to 14 mm) and slight drop in the packing density from 62 to 60% with increase MSA from No. 7 to No. 67 (14 to 20 mm).

4.5—Chemical admixtures

4.5.1 *High-range water-reducing admixtures*—Assaad and Khayat (2006a) performed a study using three types of HRWRA (polycarboxylate, polynaphthalene sulphonate, and polymelamine sulphonate) while keeping the slump constant at 26 in. (650 mm). For any given *w*/*cm*, the type of HRWRA appears to have limited effect on the initial lateral pressure. However, depending on the synergistic characteristics of the constituent materials of the HRWRAs, the pressure decay varied. Mainly, polycarboxylate-based HRWRA that had a greater fluidity retention resulted in slower pressure decay. Additionally, some HRWRAs designed to retain workability for extended periods of time can slow down the rate of structural buildup and the rate of decrease in lateral pressure without affecting the setting time (Yamada et al. 2000).

4.5.2 *Viscosity/thixotropy-modifying admixtures*—VMAs increase the yield stress and viscosity of cement-based materials and are widely available in the market. On the other hand, thixotropy-modifying admixtures (TMAs) are less widely available materials that can mainly increase yield stress at rest with limited change in viscosity (Khayat et al. 2002). VMAs can necessitate an increase in HRWRA demand. VMAs can reduce the risk of bleeding, segregation, and surface settlement through various mechanisms, including association of water with the VMA and entanglement of polymer chains of the VMA (Khayat 1998; Palacios and Flatt 2016). Alternatively, TMAs function by inducing a network structure in the liquid phase through increased interactions of the solid particles (Khayat et al. 2002), leading to an increase in stability.

Assaad and Khayat (2006b) conducted an experimental program to determine the influence of the type and concentration of VMA on form pressure exerted by SCC. Various VMA types (liquid polysaccharide-based, powder polysaccharide-based, cellulose-based) were tested along with varying dosages of HRWRA. Irrespective of the combinations tested, the results indicated that the incorporation of the VMA at low concentrations resulted in lower initial form pressure and faster pressure decay when compared to mixtures with medium or high concentrations of VMA. This effect was attributed to the increased demand of HRWRA. This study also found that the initial pressure and the pressure decay correlate to the thixotropy of the SCC mixture.

Khayat and Assaad (2008) conducted a research study that evaluated the impact of TMAs on the variation in thixotropy and their effect on lateral form pressure for mixtures with a slump flow of 25.5 ± 0.5 in. (650 ± 15 mm). The study compared the effect of using VMAs and TMAs. The results showed that mixtures containing TMA have a lower form pressure compared to similar mixtures containing VMAs. This was attributed to the higher degree of thixotropy that the mixtures with TMAs experienced. Combining a conventional VMA with TMA at low concentrations was found to be beneficial in reducing the lateral pressure as well as increasing the pressure decay compared with mixtures containing only VMA at similar concentrations.

4.5.3 *Set-modifying admixtures*—Various studies have been conducted that directly relate the form pressure exerted by SCC to the thixotropy of the mixture. Assaad et al. (2003b) investigated the relationship between pressure decay and the addition of either set-retarding admixture (RET) or set-accelerating admixture (ACC). With the addition of an RET in an SCC mixture, it was found that there was a delay in cement hydration, thus leading to a slower pressure decay in lateral pressures. This was compared to an SCC mixture proportioned with ACC, leading to an accelerated rate of hydration and faster pressure decay. In the study, both mixtures exhibited similar lateral pressures immediately after casting, but experienced significantly different pressure decay.

Table 5.1—Overall effect of casting parameters on form pressure characteristics

Increase of	Initial lateral pressure	Pressure decay	Main reason
Concrete temperature	Limited change or decrease	Faster	Accelerated rate of hydration leading to faster development of cohesion (Assaad and Khayat 2007; Omran et al. 2014)
Rate of casting	Increase	No effect observed	No stiffening allowed to reduce lateral pressure (Assaad and Khayat 2007; Omran et al. 2014)
Formwork width (thickness of concrete element)	Increase	Slower	Reduction in arching action with increasing width (Omran and Khayat 2017a)
Formwork roughness	Decrease	Information not available	Increase of friction between formwork and concrete (Djelal et al. 2002; Tchamba et al. 2008)
Reinforcement percentage	Decrease	No effect observed	Partial support from reinforcement reduces load transferred to formwork (Matar and Assaad 2017; Omran and Khayat 2017b; Perrot et al. 2009)

CHAPTER 5—EFFECT OF CASTING PARAMETERS ON FORM PRESSURE

5.1—Introduction

In addition to the SCC mixture characteristics, the casting parameters such as concrete temperature, casting rate, formwork dimensions, and reinforcement percentage also affect the initial lateral pressure and pressure decay. The effect of these parameters on form pressure and pressure decay are discussed in detail in the following subsections and are summarized in Table 5.1.

5.2—SCC mixture temperature

The effect of temperature on form pressure for conventional concrete was studied by Roby (1935), the Portland Cement Association (Rodin 1952), and Gardner (1984). Assaad and Khayat (2007) investigated the effect of concrete temperature (50, 68, and 86°F [10, 20, and 30°C]) on form pressure characteristics of SCC mixtures made with ternary binder (6% SF, 22% FA, and 72% cement) and having a *w*/*cm* of 0.4 and slump flow of 25.5 ± 0.5 in. (650 ± 15 mm). The results shown in Fig. 5.2a indicate that for lower temperatures, the rate of cement hydration is decreased, resulting in a reduced rate of pressure decay. The decrease in lateral pressure with increased concrete temperature is evident in the work of Omran et al. (2014) for an SCC mixture with a water-powder ratio (*w*/*p*) of 0.37 and slump flow of 27.5 ± 1 in. (700 ± 20 mm) shown in Fig. 5.2b.

Khayat and Omran (2010b) considered the effect of temperature on lateral pressure and proposed two different prediction models. The first model involves the measurement of thixotropy at room temperature (72 ± 4°F [22 ± 2°C]) and includes the concrete temperature as a variable in the model, as shown in Eq. (5.2a). The second model includes the thixotropy of the concrete at the target temperature, as indicated in Eq. (5.2b). Equation (5.2b) is valid in the range 53 to 86 ± 4°F (12 to 30 ± 2°C). These equations are valid for SI units.

$$P_{max}\,(\text{Pa}) = \frac{w_c g H}{100} \times \left[109.5 - 3.9H + 0.7R - 0.6T + 3D_{min} - 0.29\,PV\tau_{0rest@T=22\pm2^{\circ}\text{C}}(t)\right] \quad (5.2a)$$

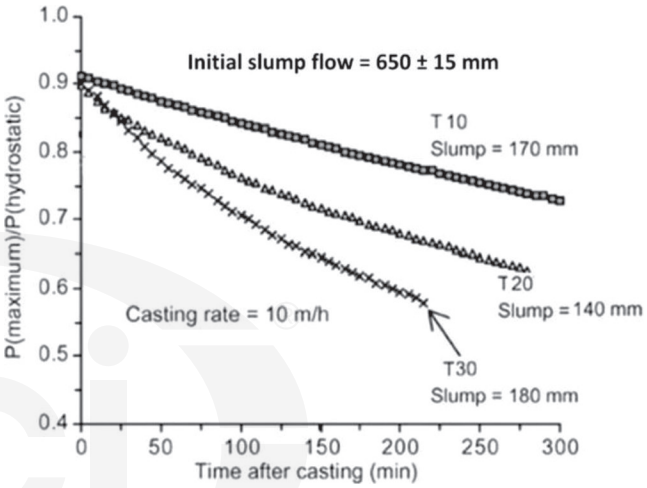

Fig. 5.2a—Effect of temperature (50, 68, and 86°F [10, 20, and 30°C]) on lateral pressure characteristics. Slump at end of pressure monitoring is noted (Assaad and Khayat 2007). (Note: 1 m = 3.3 ft; 1 mm = 0.394 in.)

$$P_{max}\,(\text{Pa}) = \frac{w_c g H}{100}\left[95.9 - 3.84H + 0.71R + 4.1D_{min} - 0.29\,PV\tau_{0rest}(t)\right] \quad (5.2b)$$

where w_c is the concrete density (unit weight) (kg/m^3); g is acceleration due gravity (m/s^2); T is the average concrete temperature (°C); H is element height (m); R is the casting rate (m/h); D_{min} is the minimum lateral dimension of the formwork (m); $PV\tau_{0rest@T=22\pm2^{\circ}\text{C}}(t)$ is the rate of gain in yield stress with time of rest (Pa/min) measured at 72 ± 4°F (22 ± 2°C) using a portable vane; and $PV\tau_{0rest}(t)$ is the rate of gain in yield stress with time of rest (Pa/min) measured at a given concrete temperature.

5.3—Casting rate

The casting rate is another critical parameter that influences the form pressure of SCC. Several investigations have been carried out to determine the influence of casting rate on the development of lateral pressure (Assaad and Khayat 2007; Beitzel and Muller 2004; Fedroff and Frosch 2004; Leemann and Hoffmann 2003; Omran et al. 2014; Tejeda-Dominguez et al. 2005; Vanhove et al. 2001). Ritchie (1962) conducted

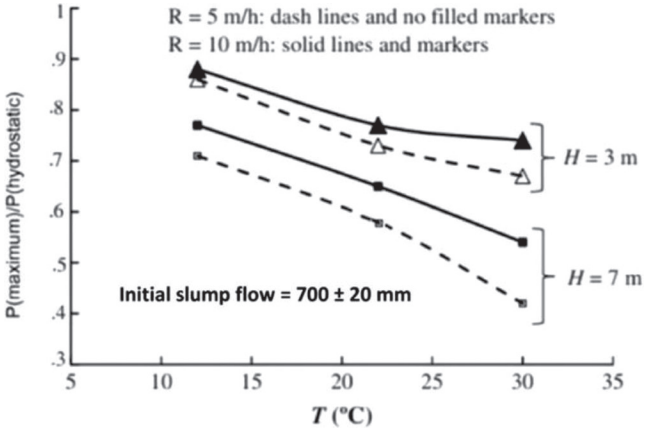

Fig. 5.2b—Effect of SCC temperature on relative lateral pressure (Omran et al. 2014). (Note: 1 m = 3.3 ft; 1 mm = 0.394 in.; T(°F) = (T(°C) × (9/5))+32.)

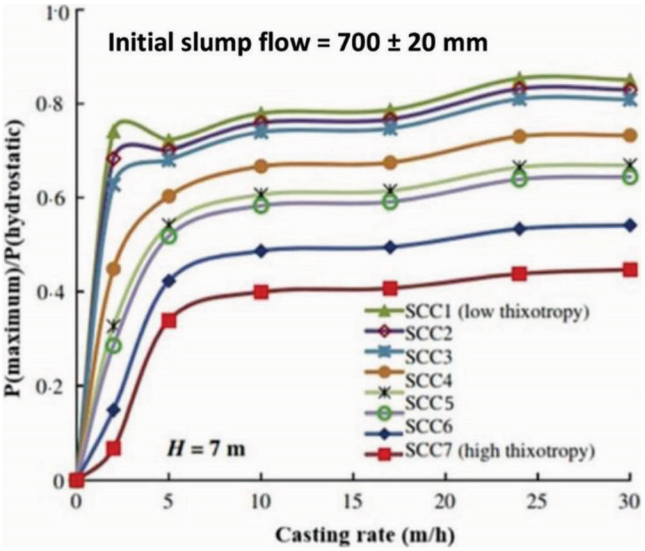

Fig. 5.3a—Effect of casting rate on relative lateral pressure (Omran et al. 2014). (Note: 1 mm = 0.394 in.; 1 m = 3.3 ft.)

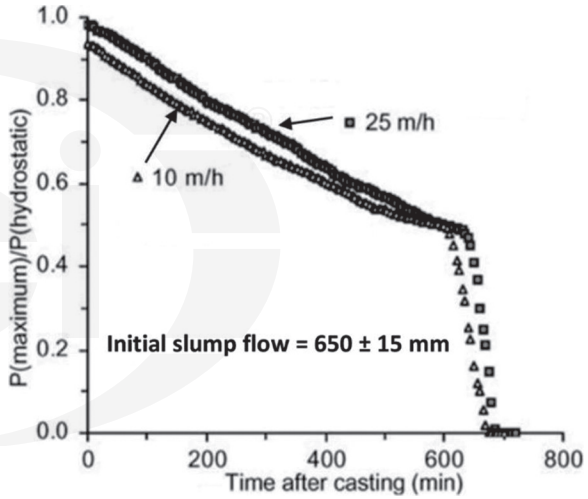

Fig. 5.3b—Effect of casting rate on lateral pressure characteristics (Assaad and Khayat 2007). (Note: 1 mm = 0.394 in.; 1 m = 3.3 ft.)

experiments on conventional concrete with varying cement-to-total-coarse-aggregate ratios with varying casting rates and found that irrespective of the composition and workability of the mixture, lateral pressure was found to increase with the casting rate. Similar results have been observed by Omran et al. (2014), shown in Fig. 5.3a for SCC mixtures with varying degrees of thixotropy and slump flow of 27.5 ± 1.0 in. (700 ± 20 mm), and by Assaad and Khayat (2007) (Fig. 5.3b) for SCC made with ternary binder (6% SF, 22% FA, and 72% cement) and have a *w*/*cm* of 0.4 and slump flow of 25.5 ± 0.5 in. (650 ± 15 mm). At faster casting rates, no structural buildup of the material occurs and the SCC form pressure can reach hydrostatic pressure. This condition typically occurs in small-volume pours that can be completed in a single lift; examples includes casting SCC for repair/strengthening applications. However, from form pressure measurements performed in larger placements where the casting rates are slower, the maximum pressure is considerably smaller than the hydrostatic pressure due to structural buildup (Assaad and Khayat 2005c; Assaad et al. 2003b; Billberg et al. 2014; Gardner et al. 2016).

The method of casting also has a significant effect on form pressure. When comparing between concrete cast from the top of the formwork and pumped from the bottom of the formwork, higher lateral pressure is exerted in the latter case. This is because the concrete is in constant motion (or shear) during pumping from the bottom. As a result, no structural buildup is allowed to happen until after placement is completed. This lack of structural buildup results in high lateral pressure that is close to full-hydrostatic pressure (Leemann and Hoffmann 2003).

5.4—Formwork characteristics

Research over the years has evaluated the effects of formwork geometry and surface roughness to determine their contribution to the overall form pressure. Rodin (1952) reported that the general trends indicate that the maximum pressure appears to be lower in form systems of smaller cross sections. This can be attributed to the increased degree of the arching effect, which reduces lateral pressure. The arching effect herein refers to the interaction between coarse aggregate particles and the formwork, reinforcement, or both. Omran and Khayat (2017a) evaluated the effect of formwork width on form pressure for SCC mixtures (SCC1 and SCC2) and the results are shown in Fig. 5.4. The SCC1 mixture is made of 5% SF, 25% SL, and 70% cement and has a slump flow of 28 in. (705 mm) and static yield stress at 15 minutes' rest is 0.11 psi (755 Pa); SCC2 is made of 5% SF, 23% FA, and 72% cement and has a slump flow of 26 in. (660 mm) and static yield stress at 15 minutes' rest is 0.05 psi (320 Pa). Omran and Khayat (2017a) observed an increase in the lateral pressure and a slower pressure decay with an increase in formwork width. With an increase in formwork width, the increase in lateral pressure was due to a reduction in the arching effect, and the slower pressure decay was due to an increase in pressure cancellation time.

Rigid and smooth formwork materials result in higher lateral pressure (Khayat and Omran 2010b). The roughness of the forms plays a role due to the dynamic friction that develops upon concrete placement. The application of demolding agents, such as form-release oil, can decrease friction and lead to an increase in lateral pressure (Djelal et al. 2002; Khayat and Omran 2010b). Tchamba et al. (2008) observed a decrease in form pressure with an increase in the surface roughness of the formwork. This was attributed to the increase in the shear stress supported by the formwork wall. Khayat et al. (2005a) also found that the surface roughness, formwork geometry, and structural buildup of the concrete mixture all play important roles in the accuracy of predicted values of the form pressure.

5.5—Reinforcement percentage

The presence of reinforcement can decrease form pressure because the reinforcement can support part of the concrete weight. Perrot et al. (2009) introduced the lateral pressure prediction model shown in Eq. (5.5a) that accounts for the effect of the reinforcement.

$$\frac{P_{max}}{P_{hydrostatic}} = 1 - \left(\frac{\varphi_b + 2S_b}{(e - S_b)\varphi_b}\right)\frac{\tau_{0rest}(t)H}{\rho g R} \tag{5.5a}$$

where

$$S_b = n_b \frac{\pi \varphi_b^{\,2}}{4} \tag{5.5b}$$

where $P_{max}/P_{hydrostatic}$ is the relative lateral pressure; φ_b is the average diameter of the vertical reinforcing bars (ft [m]); S_b is the horizontal steel section per linear foot (meter) of width (ft [m]) that corresponds to the ratio of the total cross-sectional area of the vertical reinforcing bars (ft^2 [m^2]) to the formwork width (ft [m]); n_b is the number of vertical reinforcing bars per foot (meter) of formwork length (1/ft [1/m]); e is the formwork thickness (ft [m])—that is, shortest dimension in case of a rectangular formwork; $\tau_{0rest}(t)$ is the structural buildup measured as rate of increase in yield stress with rest time (psf/min [Pa/min]); H is the height of concrete in formwork (ft [m]); ρ is the density of concrete (lb/ft^3 [kg m^3]); g is the acceleration due to gravity (ft/s^2 [m/s^2]); and R is the casting rate (ft/min [m/min]).

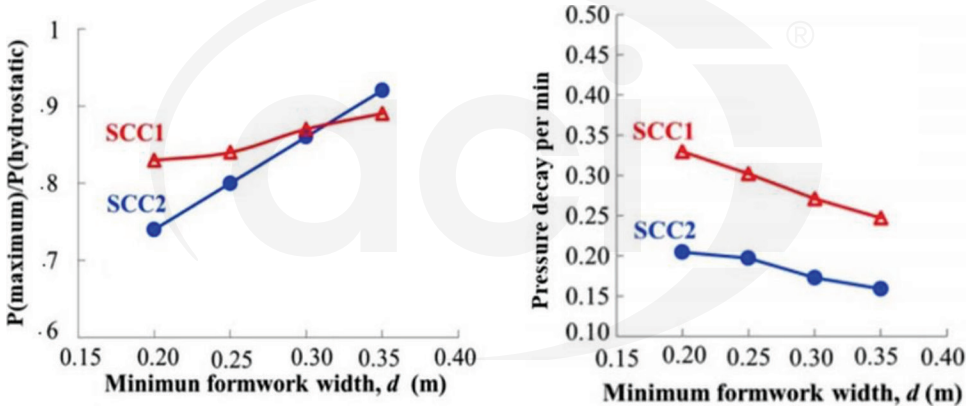

Fig. 5.4—Effect of formwork width on relative lateral pressure (left) and pressure decay (right) (Omran and Khayat 2017a). (Note: 1 mm = 0.394 in.; 1 m = 3.3 ft.)

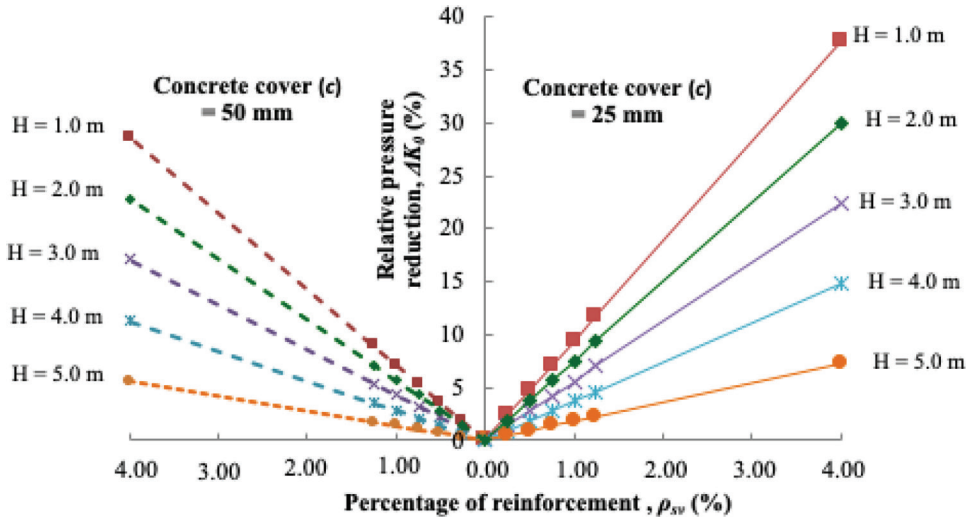

Fig. 5.5—Effect of percentage of reinforcement on lateral pressure reduction (based on Omran and Khayat 2017b). (Note: 1 mm = 0.394 in.; 1 m = 3.3 ft.)

Omran and Khayat (2017b) introduced a coefficient ($f_{\rho sv}$) that enables the reduction of the estimated lateral pressure P_{max} (ΔK_0) in sections with different reinforcement percentages (ρ_{sv}), as noted in Eq. (5.5c). The term ρ_{sv} corresponds to the cross-sectional area of vertical reinforcing bars divided by the cross-sectional area of the concrete element, expressed in percent.

$$f_{\rho sv} = 1 - \rho_{sv}\left(4.63 + \frac{4.185}{\text{concrete cover (in.)}}\right) \quad \text{(in.-lb)}$$
$$f_{\rho sv} = 1 - \rho_{sv}\left(4.63 + \frac{106.3}{\text{concrete cover (mm)}}\right) \quad \text{(SI)} \qquad (5.5c)$$

As shown in Fig. 5.5, the term $f_{\rho sv}$ varies with concrete cover and height of the cast element (H). The $f_{\rho sv}$ coefficient is applicable within the values that were used to establish this coefficient including concrete cover up to 2 in. (50 mm), $f_{\rho sv}$ up to 4%, and formwork height of up to 17 ft (5 m).

CHAPTER 6—PREDICTION MODELS FOR SCC FORM PRESSURE

6.1—Introduction

Numerous models have been developed based on theoretical principles, laboratory studies, and field studies to predict the lateral pressure exerted by SCC. Four of these models are covered in this chapter. These models mentioned herein do not take into account the reduction in form pressure due to the presence of reinforcement, which can have a substantial effect on lateral pressure, depending on the concrete cover depth and reinforcement percentage, as shown in Section 5.5. More details on such considerations can be found in Perrot et al. (2009) and Omran and Khayat (2017b).

6.2—Model by Gardner et al. (2012)

This model is based on field observations by Gardner et al. (2012) and includes the following parameters: concrete density (unit weight); w_c (lb/ft^3 [kg/m^3]) casting rate (R (ft/h [m/h]); time to fill the formwork to height H (t_H (h)), and time for the slump flow of concrete to theoretically reach zero (t_0 (h)); t_0 is considered to correspond to the time when the concrete could support its own weight. The t_0 parameter is obtained by linearly extrapolating the rate of slump flow loss, which is measured using an inverted slump cone (ASTM C1611/C1611M, Procedure B), with time to decrease to 15.75 in. (400 mm) (t_{400} (h)), as indicated in Eq. (6.2a). The lateral pressure (P_{max} (lb/ft^2 [kPa])) exerted by SCC can be calculated using Eq. (6.2b) and (6.2c). Mixtures of initial slump flow of 600 to 700 mm (24 to 28 in.) were used to develop the model. A numerical example both in inch-pound and in SI units for the prediction of the lateral pressure using this model is presented in Appendix A1.

$$t_0 = t_{15.75\text{ in.}}\left[\frac{\text{Initial slump flow (in.)}}{(\text{Initial slump flow (in.)} - 15.75)}\right] \quad \text{(in.-lb)}$$
$$t_0 = t_{400\text{ mm}}\left[\frac{\text{Initial slump flow (mm)}}{(\text{Initial slump flow (mm)} - 400)}\right] \quad \text{(SI)} \qquad (6.2a)$$

$$P_{max}\,(\text{psf}) = w_c R\left(t_H - \frac{t_H^{\,2}}{2t_0}\right) \text{ for } t_H < t_0 \quad \text{(in.-lb)}$$
$$P_{max}\,(\text{Pa}) = w_c g R\left(t_H - \frac{t_H^{\,2}}{2t_0}\right) \text{ for } t_H < t_0 \quad \text{(SI)} \qquad (6.2b)$$

$$P_{max}\,(\text{psf}) = \frac{w_c R t_0}{2} \text{ for } t_H \geq t_0 \quad \text{(in.-lb)}$$
$$P_{max}\,(\text{Pa}) = \frac{w_c g R t_0}{2} \text{ for } t_H \geq t_0 \quad \text{(SI)} \qquad (6.2c)$$

6.3—Model by Khayat and Omran (2010b)

Numerous models are established based on laboratory tests conducted using a pressure column that is 2.3 ft (0.7 m) tall and with an internal diameter of 0.7 ft (0.2 m), as shown in Fig. 6.3a. The column is designed to simulate a concrete placement height of up to 43 ft (13 m) by applying overhead pressure. The models to predict the lateral pressure are developed in SI units using linear regression analysis by fitting approximately 780 data points while taking into account the following parameters: concrete density (unit weight) (w_c [kg/m^3]); element height (H [m]); casting rate (R [m/h]); equivalent minimum lateral dimension of the formwork (D_{min} [m]) with its value changed depending on the actual minimum dimension of the formwork (d [m]), as shown in Table 6.3a; maximum size of the aggregate (MSA) (f_{MSA}); waiting period (WP) between successive lifts (f_{WP}); and SCC thixotropy.

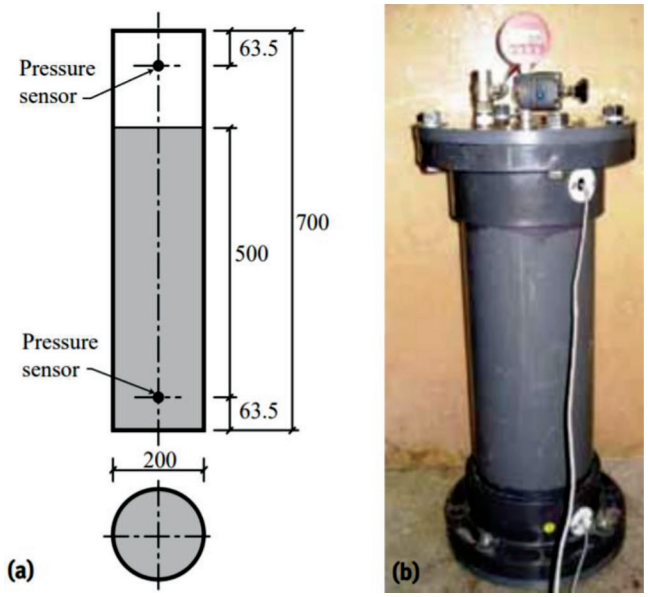

Fig. 6.3a—Portable pressure column setup (Khayat and Omran 2010b). The dimensions shown are in mm. (Note: 1 mm = 0.0394 in.)

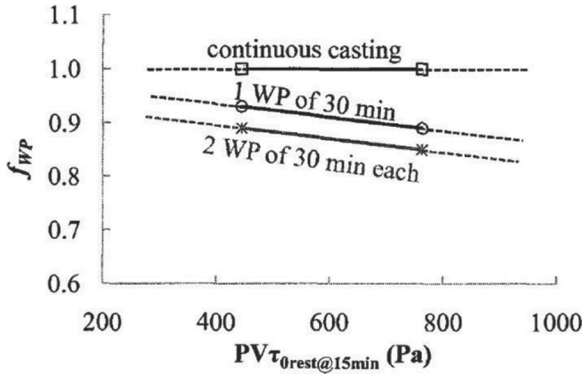

Fig. 6.3b—Correction factor of WP (Khayat and Omran 2010b). (Note: 1 Pa = 0.000145 psi.)

Table 6.3a—Equivalent minimum dimension of formwork

d	D_{min}
<0.2 m (7.9 in.)	0.2 m (7.9 in.)
0.2 m (7.9 in.) < d < 0.5 m (19.7 in.)	D
>0.5 m (19.7 in.)	0.5 m (19.7 in.)

Table 6.3b—Correction factors for MSA

$PV\tau_{0rest@15min}$, Pa	H, m	MSA, mm	f_{MSA}
≤700	<4		1
	4 to 12	20	1
		10	$1+\frac{1.26H-5.04}{100}$ *
>700	1 to 12	10 and 20	1

*The equation is in SI units, and H should be in units of meters.

Notes: The nominal MSA used are 10, 14, and 20 mm according to CAN/CSA A23.2-2A-14. Similar results can be expected with ASTM C33/C33M aggregates with nominal MSA of 9.5, 12.5, and 19.0 mm (3/8, 1/2, and 3/4 in.). 1 m = 3.3 ft; 1 mm = 0.0394 in.; 1 Pa = 0.000145 psi.

The f_{MSA} and f_{WP} values can be obtained using Table 6.3b and Fig. 6.3b, respectively. Thixotropy is measured using a portable vane, and different models are proposed based on various thixotropic indexes; that is, rate of change in the yield stress with rest time ($PV\tau_{0rest}(t)$ [Pa/min]) and yield stress after 15 minutes of rest ($PV\tau_{0rest@15min}$ [Pa]) (Khayat and Omran 2010b). The model that considers the variation in structural buildup at rest ($PV\tau_{0rest}(t)$) is presented in Eq. (6.3), and the models that consider $PV\tau_{0rest@15min}$ and the coupled effect of $PV\tau_{0rest}(t)$ and $PV\tau_{0rest@15min}$ can be found in Omran et al. (2011). The thixotropic indexes in these equations are determined at a given concrete temperature. Equation (5.2a) previously presented offers an alternative approach where the concrete temperature is a variable, and the thixotropic index is determined at 72 ± 4°F (22 ± 2°C). Further discussion on the effect of temperature on the thixotropy and form pressure is discussed by Khayat and Omran (2010b). The ranges of parameters used for these models are shown in Table 6.3c. A numerical example for the prediction of the lateral pressure using this model is presented in Appendix A2.

Table 6.3c—Parameter ranges for Khayat and Omran's model (2010b)

Parameter	Investigated ranges
Slump flow	24 to 28 in. (600 to 720 mm)
Element height (H)	3.3 to 42.6 ft (1 m to 13 m)
Concrete temperature	53 to 86 ± 4°F (12 to 30 ± 2°C)
Maximum size of the aggregate (MSA)	0.4 in. (10 mm) 0.6 in. (14 mm) 0.8 in. (20 mm)
Minimum lateral dimension of the formwork (D_{min})	8 to 14 in. (200 to 350 mm)
Waiting period between successive lifts (WP)	Continuous; 30 min WP at the middle of casting; two WPs of 30 min each at middle of casting
Rate of change in the yield stress with rest time ($PV\tau_{0rest}(t)$)	0 to 0.02 psi/min (0 to 125 Pa/min)
Yield stress after 15 minutes of rest ($PV\tau_{0rest@15min}$)	0 to 0.3 psi (0 to 2000 Pa)

$$P_{max}\,(\text{Pa}) = \frac{w_c g H}{100}\left[95.9 - 3.84H + 0.71R + 4.1D_{min} - 0.29\,PV\tau_{0rest}(t)\right] \times f_{MSA} \times f_{WP} \quad \text{(SI)} \tag{6.3}$$

6.4—Model by Tejeda-Dominguez et al. (2005)

Tejeda-Dominguez et al. (2005) developed a mathematical model for the prediction of lateral pressure exerted by SCC. The model was developed assuming that the lateral pressure is a function of the vertical pressure and shear strength of SCC. Tejeda-Dominguez et al. (2005) defined the characteristic function $C(t)$ as the ratio of lateral (P_{max}) and hydrostatic ($P_{hydrostatic}$) concrete pressures. The lateral pressure exerted during the casting of SCC is predicted by estimating the $C(t)$ using a small-scale instrumented PVC column that is 3 ft (920 mm) in length and 0.82 ft (250 mm) in diameter shown in Fig. 6.4. The test column is instrumented with flush-mounted pressure sensors installed at 0.5 ft (152 mm) from the base shown in Fig. 6.4. The sensor measures the lateral pressure exerted by concrete on the PVC column and $C(t)$ is computed as a normalized value—that is, the ratio of the lateral pressure measured and hydrostatic pressure. The computed $C(t)$ is fit with the hyperbolic function shown in Eq. (6.4a), and the variables C_0, a, and α are determined for the best-fit obtained. The values of the variables obtained from the test column are used for predicting the on-site lateral pressure using Eq. (6.4b). C_0 sets the initial value of the hyperbolic function. A value of C_0 = 1.00 indicates full-hydrostatic pressure, and this may occur if the SCC is vibrated in the test column prior to pressure measurement. However, in practice, the initial recorded pressure in the test column is slightly less than hydrostatic. Values for C_0 typically range from 0.9 to 1.0 for SCC. As general guidance, a value of C_0 = 0.95 is a reasonable assumption if measured data is not available. The values of a and α are determined

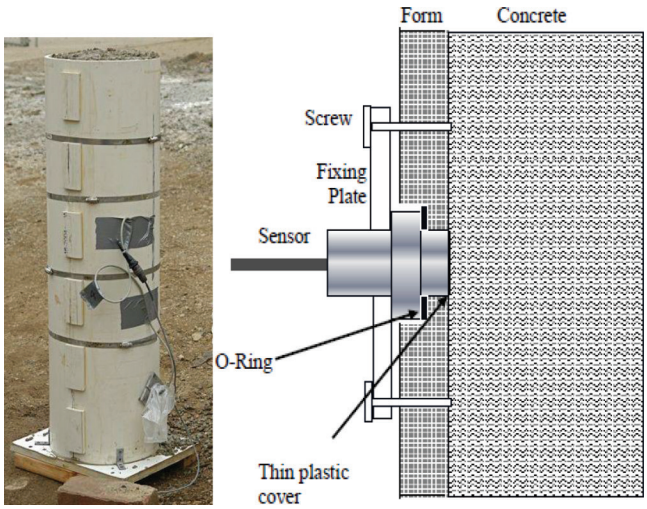

Fig. 6.4—(a) Instrumented PVC column; and (b) placement of pressure sensor in the formwork (Tejeda-Dominguez et al. 2005).

to achieve best fit between the empirical function and the experimental data. The $C(t)$ function is intended to capture the characteristic decay of pressure of the sample in the test column.

A numerical example both in inch-pound and in SI units for the prediction of the lateral pressure using this model is presented in Appendix A3.

$$C(t) = \frac{C_0}{(at^2+1)^{\alpha}} \tag{6.4a}$$

$$\begin{aligned} P_{max} &= w_c RtC(t) \quad \text{(in.-lb)} \\ P_{max} &= w_c gRtC(t) \quad \text{(SI)} \end{aligned} \tag{6.4b}$$

The maximum lateral pressure (P_{max}) occurs when the time from the start of casting (t) is

$$t = \sqrt{\frac{1}{2a(\alpha-1)}}$$

6.5—Model by Ovarlez and Roussel (2007)

Ovarlez and Roussel's (2007) model follows a theoretical approach, and it considers SCC as an elastic material confined in the formwork and follows the Tresca plasticity criterion (that is, the maximum stress sustainable by an internal plane is the yield stress of the concrete). This model uses the Janssen model (Sperl 2006) to predict the relation between the lateral (P_{max}) and hydrostatic ($P_{hydrostatic}$) concrete pressures. Ovarlez and Roussel (2007) state that the pressure exerted by concrete at a certain depth (H) is equal to a hydrostatic pressure reduced by the vertical stress at the walls, which is between 0 and the concrete yield stress at rest. It is also assumed that the weight of the concrete could cause SCC to deform vertically, and this deformation is sufficient to increase the shear stress to the yield stress of concrete. The yield stress of concrete is considered to increase linearly with time $\tau_{0rest}(t)$ (psf/h [Pa/h]), which is the case for a relatively short duration. Equation (6.5) is based on the aforementioned assumptions and considering the Janssen parameter (K) is 1. The model uses the following parameters: density (unit weight) w_c (lb/ft^3 [kg/m^3]); height H (ft [m]); width or diameter of cross section e (ft [m]); and casting rate R (ft/h [m/h]). Other details about the derivation of the equation and assumptions made can be found in Ovarlez and Roussel (2007). A numerical example both in inch-pound and in SI units for the prediction of the lateral pressure using this model is presented in Appendix A4.

$$\begin{aligned} P_{max}\,(\text{psf}) &= w_c H\left(1-\frac{H\tau_{0rest}(t)}{w_c eR}\right) \quad \text{(in.-lb)} \\ P_{max}\,(\text{Pa}) &= w_c gH\left(1-\frac{H\tau_{0rest}(t)}{w_c geR}\right) \quad \text{(SI)} \end{aligned} \tag{6.5}$$

CHAPTER 7—MEASUREMENT TECHNIQUES

There have been numerous methods developed and implemented to measure the lateral pressure exerted by fresh concrete on formwork. Brameshuber and Uebachs (2003) used a series of measuring anchors and strain measuring devices to determine the form pressure exerted by SCC. Strain gauges were also used in Cambridge-type load cells that were employed by Gardner (1984) to determine lateral pressure developed by fresh concrete. In field studies described in Chapter 8, strain-gauge-based pressure sensors were used to monitor form pressures. These pressure sensors are commercially known as flush diaphragm or millivolt-output pressure transducers, and examples of these sensors are shown in Fig. 7. The diameter of the sensor depends on the maximum size aggregate (MSA) of the mixture being monitored; the larger the aggregate, the greater the diameter, though typically for an SCC mixture, the diameters range from 0.6 to 1 in. (15 to 25 mm).

7.1—Strain-gauge-based pressure sensor setup

The measured values obtained from the sensor should be calibrated against a pressure gauge using either an oil pump or air compressor, as shown in Fig. 7.1a. The process of calibrating the sensors starts with zeroing the sensor with no applied pressure then incrementally increasing the pressure to a value slightly less than the capacity of the sensor. The voltage output of the pressure sensor is correlated with the reference pressure gauge. A pressure function for the individual sensor is then developed from the data using regression analysis.

Installation of these pressure sensors requires setting them through a drilled hole flush with the inner face of the form by means of a secured adaptor. These adaptors are not commercially available and are designed and fabricated based on each specific sensor, as they come in varying geometries based on the supplier and product type. Adaptors can be machined or 3-D printed, as shown in Fig. 7.1b, while considering their intended use: sacrificial or reusable,

Fig. 7—Examples of flush diaphragm and millivolt output pressure sensors/transducers (image courtesy of OMEGA).

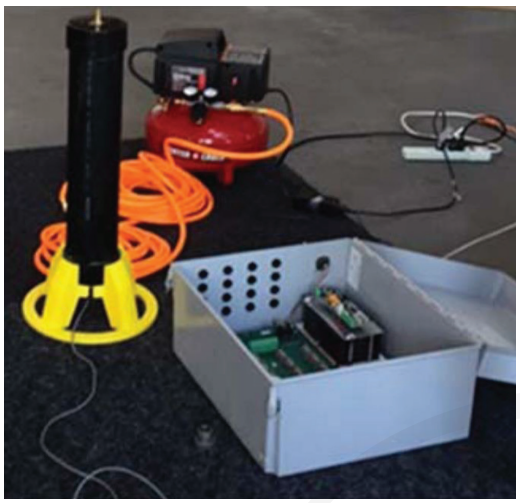

Fig. 7.1a—Calibrating pressure sensors and data acquisition system.

fixed or adjustable, form thickness, method of securing the adaptor to the form, and if spacers will be used or not.

The bottom form pressure sensor is typically installed at an elevation that is $e/2$ from the bottom of the formwork (with e being the least formwork thickness) to avoid the influence of shear restraint imposed on the fresh concrete by the bottom boundary condition. Additional sensors are installed at set intervals of approximately 3.3 ft (1 m) above the initial location to collect pressure data throughout the element height. A thin film of form-release agent or grease can be applied to the exposed face of the sensors to protect them from the concrete or, if the sensor adaptor does not require a fine-threaded seating mechanism, a thin layer of plastic wrap can be used to protect the surfaces of the sensor that will be exposed to the fresh concrete.

There are different methods, systems, and programs for reading the information relayed by the sensors. The system's pressure results can either be physically recorded on a USB and then transferred to a computer or it can be wirelessly transmitted in real time to allow the data to be viewed as placement progresses, as shown in Fig. 7.1c. Once the sensors are installed, and prior to casting the concrete, there may be initial pressure readings due to the loss of rebound since its last use or due to factors such as differences in atmospheric pressure. If the formwork pressure is being monitored in real time, those initial readings must either be set to zero, if possible, or be recorded and subtracted from

Fig. 7.1b—Pressure sensor adaptors.

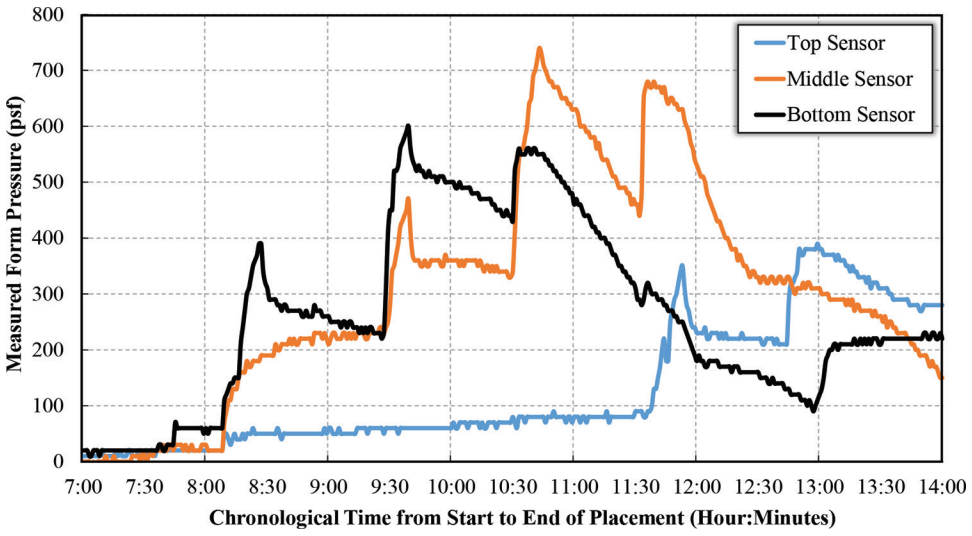

Fig. 7.1c—Measured pressure versus chronological time of placement. (Note: 1 psf = 47.88 Pa.)

later results to effectively analyze the data. In all cases, any initial readings must be subtracted from subsequent results when analyzing the data.

7.2—Pressure reading graph example

Figure 7.1c shows a typical graph of measured results for lateral pressure that can be established by using a pressure transducer measurement system in the field. The example presented was from a large core placement on a high-rise construction project in Toronto. The total height of the self-climbing formwork system was 19.7 ft (6.0 m), or 1.5 stories per lift. Casting was done in the summer where temperatures were approximately 86°F (30°C). The casting rate was 3.3 ft /h (1.0 m/h) for a total placing time of 6 hours. Three sensors were located at varying heights (bottom, middle, and top) in a vertical line at a specific formwork panel location. The vertical (y) axis is the measured lateral formwork pressure, and the horizontal (x) axis is the chronological time from the start to the end of concrete placement. Each pressure transducer is shown to record the lateral pressure of the concrete relative to its vertical location in the formwork. At the start of placement, the first cell to show a pressure increase is the bottom sensor or the black line, the second sensor showing an increase in pressure is the middle sensor or the orange line, and finally, the last to show pressure increase is the top sensor or the blue line. The bottom sensor and the middle sensor were spaced 3.3 ft (1 m) apart vertically, and the top sensor was spaced 3.3 ft (1 m) vertically from the middle sensor. The spike in the measured pressure shown for each sensor occurs when an additional lift of concrete is placed. The impact of time and thixotropy on the lateral formwork pressure can be clearly seen in the measured results shown for the bottom sensor in Fig. 7.1c. Note that the measured formwork pressure immediately increases as a concrete lift is cast, and then the formwork pressure subsequently decays after placement. At the bottom sensor location, the maximum formwork pressure is measured when the second lift is placed, and with subsequent lifts, a reduced impact on lateral pressure can be seen, as the measured pressure is less for the third lift and most obviously for the fourth lift, where the change in pressure is minimal.

Once the concrete has set and the hydration cycle evolves, the resulting thermal expansion of the concrete against the forms and the exposed diaphragm surface of the pressure transducer could result in a large, localized pressure reading, especially in thick sections, which is not a function of plastic concrete lateral pressure. It is beneficial for the serviceability of the sensor to remove the pressure cells from their adaptor locations once the placement has been completed and prior to a large rise in pressure due to the exothermic reaction of the hydrating concrete.

7.3—Precautions and maintenance when measuring form pressure

Pressure sensors and data loggers are sensitive instruments that are susceptible to inaccurate results and irreversible damage if mishandled. The pressure sensors are manufactured to perform within a designated range of temperatures. For the types that have typically been used in formwork pressure monitoring, the operating temperature ranges are from –58 to 212°F (–50 to 100°C). It is important to ensure that the sensors will perform under the range of temperatures that will be expected during the placing and casting of the concrete elements. When setting up the equipment, a competent individual responsible for installing the sensors and connecting the data logger should be identified. It should be ensured that the sensors are correctly installed in the adaptors, as their misalignment may impact measured results. Avoid twisting of the sensor's cord and any physical damage to the sensor's diaphragm, as this may damage the internal electronics and hardware. Where applicable, do not remove or damage the ferrite bead from the sensor's cord, shown in Fig. 7, as it suppresses high-frequency noise. Finally, a safe location to store the data logger should be determined to protect it from environmental factors and physical damage.

There are also typical maintenance considerations that are expected when measuring form pressure. All equipment should be checked for physical damage and tested before use. Pressure sensors should be recalibrated at least on a yearly basis, or as per the manufacturer's recommendation, and immediately if physical damage or inconsistency in the readings are observed. Lastly, prior to setting up on site, have replacement adaptors and gaskets on hand, as they can be damaged during installation, and that either the data logger's battery is fully charged or that there is a continuous supply of electricity available to power the pressure measurement instrumentation.

CHAPTER 8—FIELD VALIDATION OF PREDICTION MODELS

Two full-scale field studies were conducted to validate the prediction models discussed in Chapter 6 (Billberg et al. 2014; Gardner et al. 2016). The details regarding the mixture designs, field tests conducted, and the measured and predicted pressure data are presented in the following.

8.1—Stockholm, Sweden, 2012

Full-scale testing was conducted in Stockholm, Sweden, to evaluate various existing form pressure models (Billberg

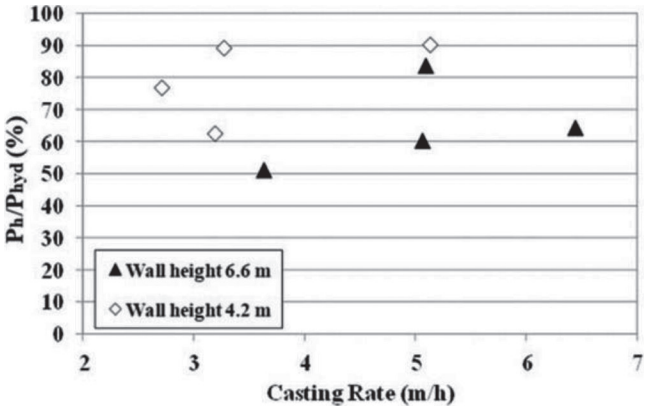

Fig. 8.1a—Casting rate and maximum relative form pressure (P_h/P_{hyd}) for all eight walls (Billberg et al. 2014). (Note: 1 m = 3.3 ft.)

Fig. 8.1b—Concrete characterization using slump flow loss test.

et al. 2014). A total of eight walls were cast using two SCC mixtures with different levels of structural buildup at rest. The dimensions of the eight walls are as follows: four walls (Walls 1, 3, 5, and 7) were 21.7 ft (6.6 m) in height, 7.9 ft (2.4 m) in length, and 7.9 in. (0.2 m) in thickness. Three other walls (Walls 2, 4, and 6) were 13.8 ft (4.2 m) in height, 7.9 ft (2.4 m) in length, and 7.9 in. (0.2 m) in thickness. One wall (Wall 8) was 13.8 ft (4.2 m) in height, 7.9 ft (2.4 m) in length, and 15.7 in. (0.4 m) in thickness. A more thixotropic mixture was used for casting Walls 1, 2, 5, 6, 7, and 8, while a low thixotropic mixture was used for casting Walls 3 and 4. The casting was done stepwise in relatively small but frequent steps to enable continuous placement of concrete in the form. A laser meter was used to measure the rising of the concrete level with time, and the casting rate was measured

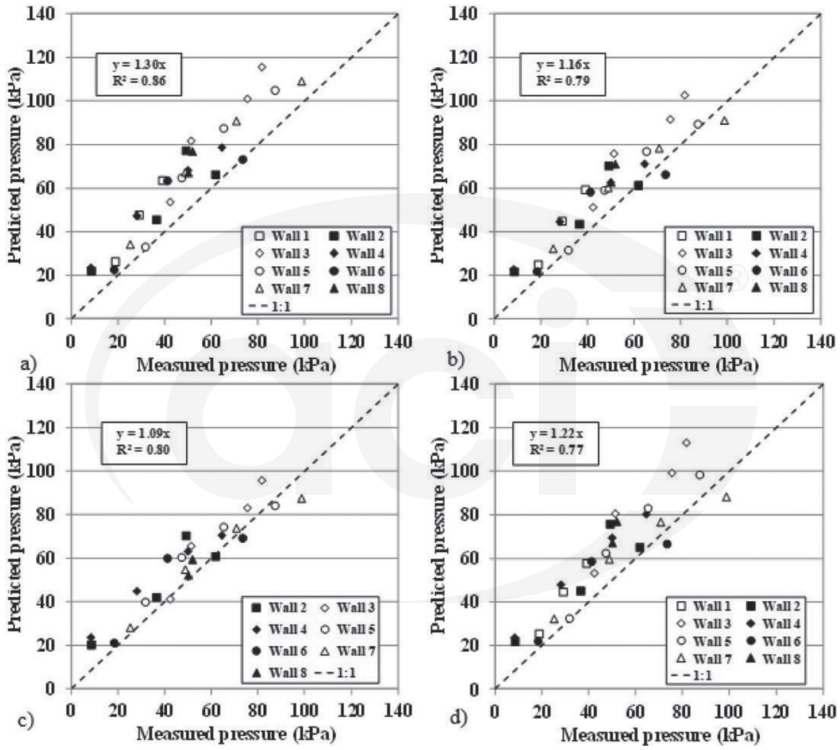

Fig. 8.1c—Predicted versus measured pressures for: (a) Gardner et al. (2012); (b) Khayat and Omran (2010b); (c) Tejeda-Dominguez et al. (2005); and (d) Ovarlez and Roussel (2007) (Billberg et al. 2014). (Note: 1 kPa = 0.145 psi.)

Table 8.1—Key parameters related to models in Chapter 6 (adapted from Billberg et al. [2014])

Model	Parameter	Wall No.							
		1*	2†	3*	4†	5*	6†	7*	8‡
Gardner et al. (2012)	t_0, h	4.0	9.7	4.2	11.3	6.6	8.3	9.3	8.2
Khayat and Omran (2010)	$PV\tau_{0rest@15min}$, Pa	410	176	261	215	307	254	319	294
	$PV\tau_{0rest}(t)$, Pa/min	16.0	5.8	9.9	2.3	11.2	9.6	18.5	9.1
Tejeda-Dominguez et al. (2005)	C_0	—	0.94	0.86	1.04	0.90	0.90	0.84	0.87
	α	—	12	12	12	12	12	12	12
	a	—	0.32	0.40	0.80	0.75	0.40	0.70	0.50
Ovarlez and Roussel (2007)	$PV\tau_{0rest}(t)$, Pa/min	16.0	5.8	9.9	2.3	11.2	9.6	18.5	9.1

*Wall dimensions (L x B x H) = 7.9 ft x 7.9 in. x 21.7 ft (2.4 x 0.2 x 6.6 m)

†Wall dimensions (L x B x H) = 7.9 ft x 7.9 in. x 13.8 ft (2.4 x 0.2 x 4.2 m)

‡Wall dimensions (L x B x H) = 7.9 ft x 15.7 in. x 13.8 ft (2.4 x 0.4 x 4.2 m)

Note: 1 Pa = 0.000145 psi; 1 Pa/min = 0.000145 psi/min.

to be between 8.8 and 21 ft/h (2.7 and 6.4 m/h). The lateral pressure was measured for each wall at different elevations using pressure sensors flush-mounted to vertical formwork surfaces. The maximum relative pressure and the casting rates measured for each wall are shown in Fig. 8.1a.

The key parameters needed for prediction of the maximum lateral pressure are measured using the portable vane shown in Fig. 3.2.1b, Lange's static column (Fig. 6.4(a)), and the slump flow loss test (Fig. 8.1b), and the results are shown in Table 8.1. Using these parameters, the maximum lateral pressure for each wall was estimated, and these values were compared to the measured lateral pressures, as shown in Fig. 8.1c. The slope of the trend lines varies between 1.09 and 1.30, and regression coefficients (R^2) are between 0.77 and 0.86. Slope values greater than 1 indicate that the estimated pressure is greater than the measured ones, and high R^2 values for all four models indicate that they can accurately predict the measured lateral pressure.

8.2—Toronto, Canada, 2014

Full-scale testing was conducted at a concrete production plant in Toronto, ON, Canada (Gardner et al. 2016). Eight columns with dimensions of 20 ft (6.1 m) in height and a cross section of 2 x 2 ft (0.61 x 0.61 m) were cast. The casting rate, reinforcement percentage (note that the reinforcement percentage for the Toronto trials was significantly less [1/10] of what would be considered typical in production elements), and SCC thixotropy were varied. The lateral pressure was measured at different elevations using pressure sensors similar to those employed for the Stockholm project.

To minimize lateral pressure effects due to the impact of falling concrete, seven of the eight columns were placed using a modified tremie. The system comprised an 8 in. (200 mm) diameter flexible PVC tube fastened to a hopper extending to approximately 15.75 in. (400 mm) from the bottom of the column. Ports measuring 6 x 4 in. (150 x 100 mm) were cut into alternating sides of the tube along its length, as shown in Fig. 8.2a. A crane and bucket were used to fill the hopper at specified intervals to match the appropriate casting rate with the exception of Column 7, which was pumped from the base at 167 ft/h (51 m/h). Pressure sensors were mounted with the sensor face flush to the surface of the formwork at varying elevations. The maximum pressure values measured

Fig. 8.2a—Modified tremie.

Table 8.2a—Summary of maximum pressure values measured at each elevation, in kPa (Gardner et al. 2016)

Gauge elevation, m			0.2	0.5	1	2	3	3.8
Concrete head, m			5.8	5.5	5	4	3	2.2
Column	*R*, m/h	Reinforcement*						
1	5.5	Dense	116.6	116.6	107.3	88.7	—	56
		Sparse	121.3	—	112	84	65.3	56
2	5	Dense	102.2	105.4	97.9	93.1	72.8	54.2
		Sparse	98	98	93.3	70	65.5	53.3
3	3	Dense	80.9	—	84.7	—	75.1	—
		Sparse	80.9	—	86.2	—	81.8	—
4	5	Dense	93.3	98	84	65.3	56	46.6
		Sparse	98	114.3	86.3	70	65.3	—
5	9.7	Dense	93.3	107.5	88.6	79.3	56	46.7
		Sparse	101.1	99.1	101.5	74.7	70	—
6	9.5	Dense	106.5	—	100.8	87.2	78.1	—
		Sparse	118	—	100.2	90.2	72	—
7	51 (pumped from base)	Dense	144.7	135.4	116.7	93.4	79.4	51.3
		Sparse	—	135.4	123.7	98	70	42
8	3	Dense	31.6	—	82.6	76.7	60.4	—
		Sparse	83.6	—	—	92.3	60.8	—

*Dense reinforcement: Nine No. 9 (30M) reinforcing bar at 2 in. (50 mm) cover. Sparse reinforcement: Two No. 5 (15M) reinforcing bar at 8 in. (200 mm) cover.

Note: 1 m = 3.3 ft; 1 kPa = 0.145 psi.

Table 8.2b—Concrete characterization results (Gardner et al. 2016)

Column	Thixotropy	Portable vane		Inclined plane	Vane rheometer (ICAR)	Tejeda-Dominguez et al. (2005) static column		Time at zero slump flow, h
		15 minutes, Pa	Slope, Pa/m	15 minutes, Pa	Slope, Pa/min	Coefficients		
						a	α	
1	Medium	820	41	390	—	0.30	0.12	3.17
2	High	1030	40	590	53	0.17	0.26	2.95
3	High	1630	24	70	46	0.92	0.08	2.62
4	Low	540	7	270	8	0.30	0.65	4.15
5	High	2050	51	520	53	—	—	2.00
6	High	2190	35	590	79	0.75	0.13	1.37
7	High	1460	36	230	40	0.82	0.17	3.53
8	High	1460	17	310	48	0.53	0.15	2.68

Note: 1 Pa = 0.000145 psi; 1 Pa/min = 0.000145 psi/min.

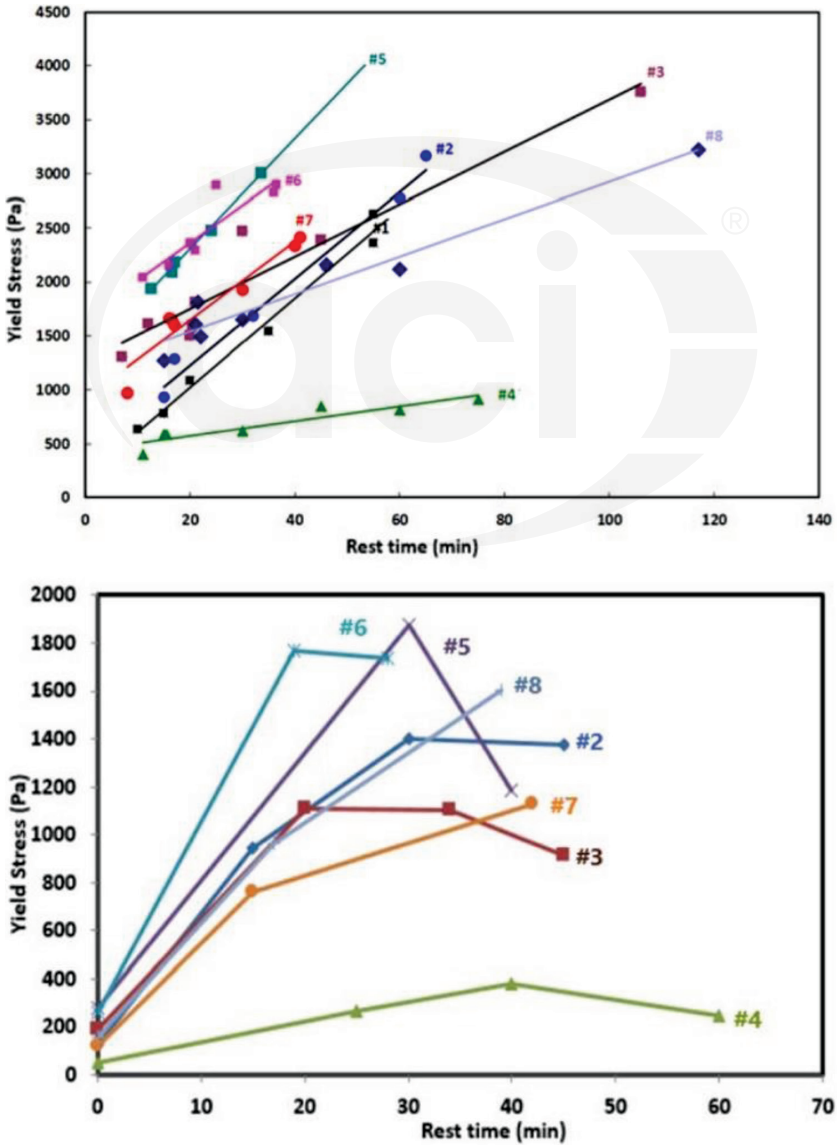

Fig. 8.2b—Concrete characterization results using portable vane (top) and ICAR (bottom) (Gardner et al. 2016). (Note: 1 Pa = 0.000145 psi.)

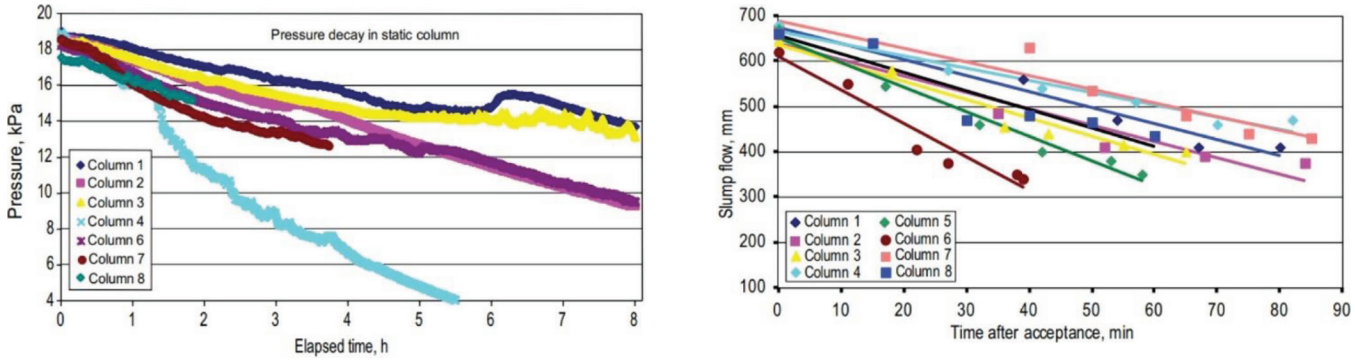

Fig. 8.2c—Concrete characterization results using Lange's static column (left) and slump cone (right) (Gardner et al. 2016). (Note: 1 kPa = 0.145 psi; 1 mm = 0.0394 in.)

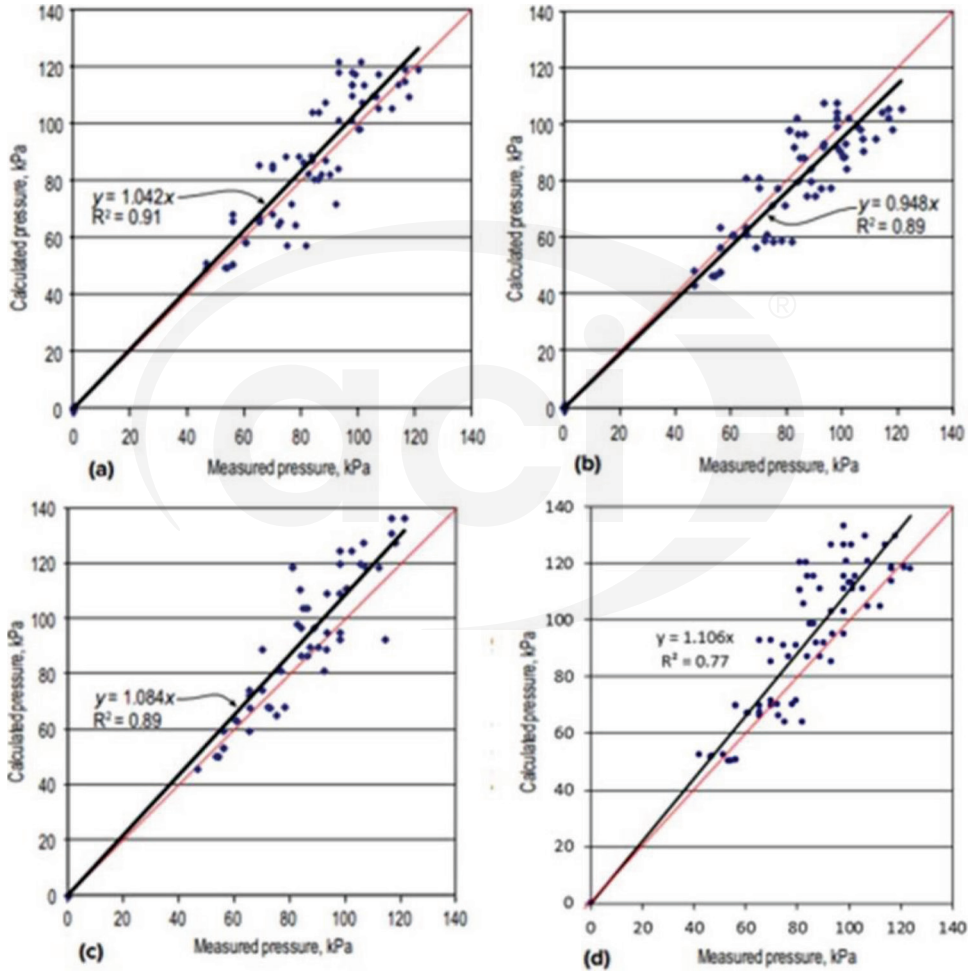

Fig. 8.2d—Measured versus predicted lateral pressures using: (a) Gardner et al. model (2012); (b) Khayat and Omran's (2010b) model; (c) Tejeda-Dominguez et al. (2005) model; and (d) Ovarlez and Roussel (2007) model (Gardner et al. 2016). (Note: 1 kPa = 0.145 psi.)

at each elevation with the sensors mounted at the sparse and dense reinforcement locations are reported in Table 8.2a.

Concrete mixtures with varying thixotropy levels were developed in laboratory tests. During the program, concrete acceptance was based on slump flow and time required for SCC to spread to a diameter of 20 in. (500 mm) (ASTM C1611/C1611M) target ranges. Thixotropy was determined using the portable vane method at 15 minutes. Low-thixotropy mixtures were defined as having shear strength below 0.10 psi (700 Pa) and high-thixotropy mixtures were defined as having shear strength greater than 0.18 psi (1250 Pa). Concrete characterization to evaluate structural buildup at rest was performed using the portable vane (Fig. 3.2.1b) and the inclined plane method (Fig. 3.2.1d),

Lange's static column (Fig. 6.4(a)), and the slump flow loss test (Fig. 8.1b), and the results are shown in Table 8.2b, Fig. 8.2b, and Fig. 8.2c. Each of the prediction models used one or more of the concrete characterization test results. These characterization test results are independent of the prediction models, but the prediction models are not independent of the characterization test results. The predicted pressure versus the measured pressure results are shown in Fig. 8.2d.

The measured lateral pressures were predicted using each of the methods described. It is important to note that the column sections were relatively small (2.9 yd^3 [2.25 m^3] concrete per column) so that even though the level of thixotropy affects the lateral pressures, the heights of the columns (20 ft [6 m]), and relatively high rates of concrete placement prevented it from being pronounced in these results.

8.3—Validation of models

The results using the Gardner et al. (2012), Khayat and Omran (2010b), Tejeda-Dominguez et al. (2005), and Ovarlez and Roussel (2007) models from the Stockholm 2012 and Toronto 2014 field studies are shown in Fig. 8.3(a), (b), (c), and (d), respectively. The plots are derived from 78 to 103 data points (N), and the standard error of the estimates are also noted in Fig. 8.3.

The trend-line equations and standard error of the estimates are shown in Fig. 8.3 and indicate that these models can be used to predict the mean measured lateral pressure with an accuracy ranging from –2% to +12%, and a standard error of the estimates ranging approximately between 1.7 to 2 psi (12 to 14 kPa). The –2% and +12% error correspond to underestimation and overestimation of measured pressures, respectively. The standard error of the estimate (S), as defined in Eq. (8.3), represents the average distance that the predicted pressure values (Y) fall from the best-fit line, shown in red. A smaller value of S indicates that predicted values are closer to the best-fit line.

$$\text{standard error of the estimate } (S) = \sqrt{\frac{\Sigma(Y - Y')^2}{N - 2}} \qquad (8.3)$$

where Y' indicates predicted pressure from best-fit line for a given value of measured pressure (X).

The four experimentally-based models can predict lateral pressure with reasonable accuracy. However, the models do not include any correction factor and safety factor. Such

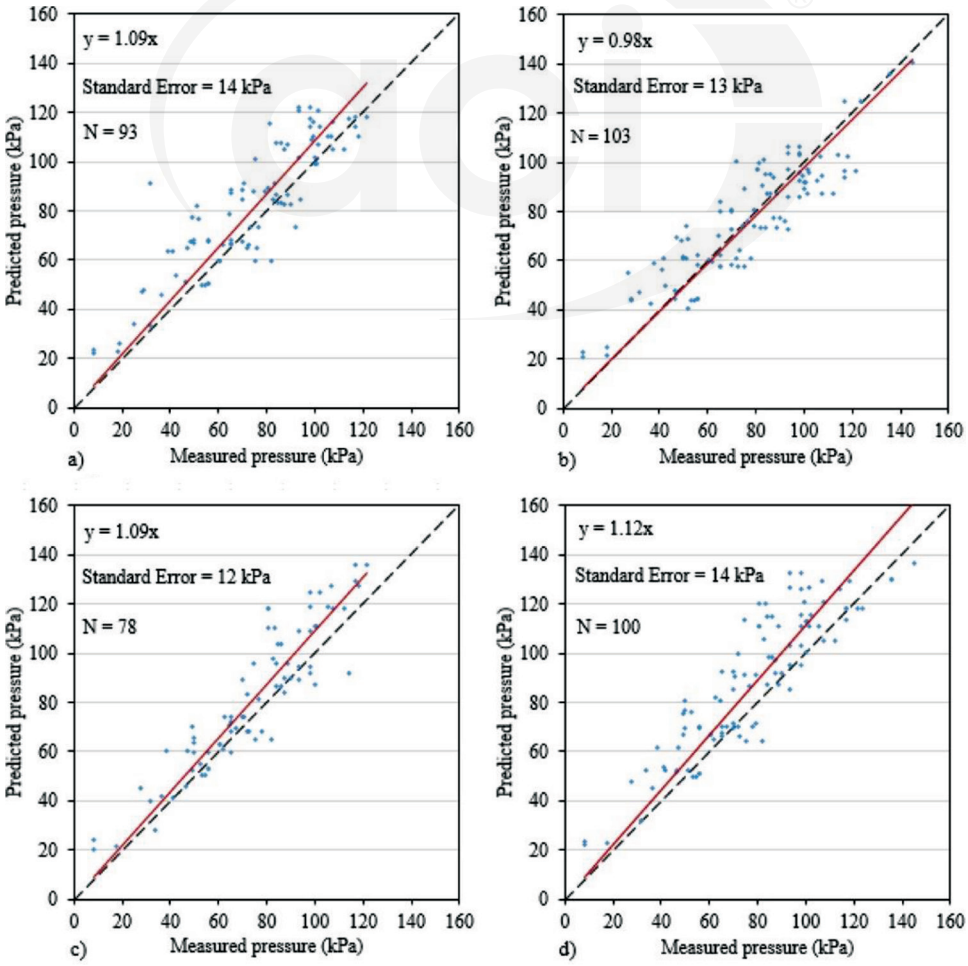

Fig. 8.3—Measured versus predicted lateral pressure from Stockholm and Toronto studies: (a) Gardner et al. model (2012); (b) Khayat and Omran (2010b) model; (c) Tejeda-Dominguez et al. (2005) model; and (d) Ovarlez and Roussel (2007) model. (Note: 1 kPa = 0.145 psi.)

factors should be applied to mean predicted pressures to obtain design values that provide conservative estimates of form pressure.

8.4—Considerations for formwork design

The development of factors of safety for use in formwork design, including those used for ASD and LRFD methodologies, is outside of the scope of this report. The correction factors or safety factors will be dependent upon the capability of the ready mixed concrete producer to control the rheological parameters (and workability tolerances, such as those based on ASTM C1611/C1611M: slump flow, T50 (time it takes for slump flow to reach a diameter of 500 mm [20 in.]), and visual stability index [VSI]) of the SCC mixture. Site personnel should also understand the variations in these parameters so that a decision for acceptance or rejection of a batch of concrete can be assessed prior to casting into forms that are designed for pressures less than hydrostatic pressure. When approaching critical pressure, the placing rate should be reduced until the pressure decay rate is such that the lateral pressure does not jeopardize formwork capacity.

It is important to note that the models and the field validations that are presented herein are suitable for applications involving open forms. However, these models may not be suitable for formed applications in highly confined areas, such as in the case of concrete enlargement applications, where lateral pressure can be higher. In the case of concrete pumped from the bottom of the formwork, ACI 347R recommends designing formwork for the full concrete hydrostatic head plus a minimum allowance of 25% for pump surge pressure.

CHAPTER 9—SUMMARY

Thixotropy (structural buildup at rest) can significantly affect the maximum lateral pressure exerted by SCC and the pressure decay. As discussed in this report, form pressure characteristics are highly influenced by constituent materials, including binder composition and chemical admixture types and combinations, and mixture proportioning. The concrete temperature, casting rate, reinforcement percentage, and formwork material and dimensions also have a significant effect on form pressure characteristics. The four experimental models presented to predict lateral pressure are based on measured thixotropic characteristics. It is important to note that these models require testing, both during mixture development and at the point of placement, to ensure that the predicted pressures are not exceeded during actual concrete placement.

It is also important to keep in mind that the experimental models are not design models. It is outside of the scope of this document to make design recommendations for formwork placed with SCC. It is recommended that the reader consult the latest design recommendations published by ACI Committee 347.

CHAPTER 10—REFERENCES

Committee documents are listed first by document number and year of publication followed by authored documents listed alphabetically.

American Concrete Institute

ACI 237R-07(19)—Self-Consolidating Concrete

ACI 238.2T-14—Concrete Thixotropy

ACI 318-19—Building Code Requirements for Structural Concrete and Commentary

ACI 347R-14—Guide to Formwork for Concrete

ACI SP-4(14)—Formwork for Concrete

ASTM International

ASTM C33/C33M-18—Standard Specification for Concrete Aggregates

ASTM C1611/C1611M-18—Standard Test Method for Slump Flow of Self-Consolidating Concrete

Canadian Standards Association

CAN/CSA-A23.2-2A-14—Sieve Analysis of Fine and Coarse Aggregate

Authored references

Alexandridis, A., and Gardner, J., 1981, "Mechanical Behaviour of Fresh Concrete," *Cement and Concrete Research*, V. 11, No. 3, pp. 323-339. doi: 10.1016/0008-8846(81)90105-8

Amziane, S., and Baudeau, P., 2000, "Effects of Aggregate Concentration and Size in Fresh Concrete Pressure on Formwork Walls," *Materials and Structures*, V. 33, No. 1, pp. 50-58. doi: 10.1007/BF02481696

Amziane, S.; Perrot, A.; and Lecompte, T., 2008, "A Novel Settling and Structural Buildup Measurement Method," *Measurement Science & Technology*, V. 19, No. 10, p. 105702 doi: 10.1088/0957-0233/19/10/105702

Andreas, L., and Frank, W., 2005, "Influence of the Mixture Design on the Formwork Pressure of Self-Compacting Concrete," *Proceedings of the 2nd North American Conf on the Design and Use of Self-Consolidating Concrete (SCC) and the 4th International RILEM Symposium on Self-Compacting Concrete*, pp. 635-640.

Arslan, M.; Şimşek, O.; and Subaşı, S., 2005, "Effects of Formwork Surface Materials on Concrete Lateral Pressure," *Construction & Building Materials*, V. 19, No. 4, pp. 319-325. doi: 10.1016/j.conbuildmat.2004.07.007

Assaad, J., 2004, "Formwork Pressure of Self-consolidating Concrete: Influence of Thixotropy," University of Sherbrooke, Sherbrooke, QC, Canada, 453 pp.

Assaad, J., and Khayat, K., 2004, "Influence of Internal Friction and Cohesion on the Variations of Formwork Pressure of Self-Consolidating Concrete," *Seventh CANMET/ACI International Conference on Recent Advances in Concrete Technology*, SP-222, American Concrete Institute, Farmington Hills, MI, pp. 19-32.

Assaad, J., and Khayat, K., 2005a, "Effect of Coarse Aggregate Characteristics on Lateral Pressure Exerted by

Self-Consolidating Concrete," *ACI Materials Journal*, V. 102, No. 3, May-June, pp. 145-153.

Assaad, J., and Khayat, K., 2005b, "Formwork Pressure of Self-Consolidating Concrete Made with Various Binder Types and Contents," *ACI Materials Journal*, V. 102, No. 4, July-Aug., pp. 215-223.

Assaad, J., and Khayat, K., 2005c, "Kinetics of Formwork Pressure Drop of Self-Consolidating Concrete Containing Various Types and Contents of Binder," *Cement and Concrete Research*, V. 35, No. 8, pp. 1522-1530. doi: 10.1016/j.cemconres.2004.12.005

Assaad, J., and Khayat, K., 2006a, "Effect of Mixture Consistency on Formwork Pressure Exerted by Highly Flowable Concrete," *Journal of Materials in Civil Engineering*, V. 18, No. 6, pp. 786-791. doi: 10.1061/(ASCE)0899-1561(2006)18:6(786)

Assaad, J., and Khayat, K., 2006b, "Effect of Viscosity-Enhancing Admixtures on Formwork Pressure and Thixotropy of Self-Consolidating Concrete," *ACI Materials Journal*, V. 103, No. 4, July-Aug., pp. 280-287.

Assaad, J., and Khayat, K., 2007, "Effect of Casting Rate and Concrete Temperature on Formwork Pressure of Self-Consolidating Concrete," *Materials and Structures*, V. 39, No. 3, pp. 333-341. doi: 10.1007/s11527-005-9042-3

Assaad, J.; Khayat, K.; and Mesbah, H., 2003a, "Assessment of Thixotropy of Flowable and Self-Consolidating Concrete," *ACI Materials Journal*, V. 100, No. 2, pp. 99-107.

Assaad, J.; Khayat, K.; and Mesbah, H., 2003b, "Variation of Formwork Pressure with Thixotropy of Self-Consolidating Concrete," *ACI Materials Journal*, V. 100, No. 1, pp. 29-37.

Barnes, H., 1997, "Thixotropy—A Review," *Journal of Non-Newtonian Fluid Mechanics*, V. 70, No. 1-2, pp. 1-33. doi: 10.1016/S0377-0257(97)00004-9

Beitzel, M., and Muller, H., 2004, "Modeling Fresh Concrete Pressure on Vertical Formwork," *Proceedings of the 5th International Ph D Symposium in Civil Engineering*, pp. 1-6.

Billberg, P., 2006, "Form Pressure Generated by Self-Compacting Concrete: Influence of Thixotropy and Structural Behaviour at Rest," *Royal Institute of Technology, Stockholm, Sweden,* 86 pp.

Billberg, P.; Roussel, N.; Amziane, S.; Beitzel, M.; Charitou, G.; Freund, B.; Gardner, J. N.; Grampeix, G.; Graubner, C.-A.; Keller, L.; Khayat, K. H.; Lange, D. A.; Omran, A. F.; Perrot, A.; Proske, T.; Quattrociocchi, R.; and Vanhove, Y., 2014, "Field Validation of Models for Predicting Lateral Form Pressure Exerted by SCC," *Cement and Concrete Composites*, V. 54, pp. 70-79. doi: 10.1016/j.cemconcomp.2014.02.003

Brameshuber, W., and Uebachs, S., 2003, "Investigations on the Formwork Pressure Using Self-Compacting Concrete," *Self-Compacting Concrete: Proceedings of the 3rd International RILEM Symposium (PRO33)*, RILEM, Paris, pp. 281-287.

Djelal, C.; Vanhove, Y.; De Caro, P.; and Magnin, A., 2002, "Role of Demoulding Agents During Self-Compacting Concrete Casting in Formwork," *Materials and Structures*, V. 35, No. 8, pp. 470-476. doi: 10.1007/BF02483134

Dzuy, N. Q., and Boger, D. V., 1985, "Direct Yield Stress Measurement with the Vane Method," *Journal of Rheology (New York, N.Y.)*, V. 29, No. 3, pp. 335-347. doi: 10.1122/1.549794

Fedroff, D., and Frosch, R., 2004, "Formwork for Self-Consolidating Concrete," *Concrete International*, V. 26, No. 10, pp. 32-37.

Gardner, J., 1984, "Formwork Pressures and Cement Replacement by Fly Ash," *Concrete International*, V. 6, No. 10, pp. 50-55.

Gardner, J.; Keller, L.; Khayat, K.; Lange, D.; and Omran, A., 2016, "Field Measurements of SCC Lateral Pressure—Toronto 2014," *Concrete International*, V. 38, No. 6, pp. 42-50.

Gardner, J.; Keller, L.; Quattrociocchi, R.; and Charitou, G., 2012, "Field Investigation of Formwork Pressures Using Self-Consolidating Concrete," *Concrete International*, V. 34, No. 1, pp. 41-47.

Ghezal, A.; Kamal, K.; and Beaupré, D., 2002, "Effect of High-Range Water-Reducer/Viscosity-Modifying Admixture Combination on Rheological Properties of Concrete Equivalent Mortar," *Proceedings of the First North American Conference on the Design and Use of Self-Consolidating Concrete*, pp. 159-165.

Ghio, V.; Monteiro, P.; and Demsetz, L., 1994, "The Rheology of Fresh Cement Paste Containing Polysaccharide Gums," *Cement and Concrete Research*, V. 24, No. 2, pp. 243-249. doi: 10.1016/0008-8846(94)90049-3

Ish-Shalom, M., and Greenberg, S., 1960, "The Rheology of Fresh Portland Cement Pastes," *4th International Symposium on Chemistry of Cement*

Khayat, K., 1998, "Viscosity-Enhancing Admixtures for Cement-Based Materials—an Overview," *Cement and Concrete Composites*, V. 20, No. 2-3, pp. 171-188. doi: 10.1016/S0958-9465(98)80006-1

Khayat, K., and Assaad, J., 2005, "Use of Rheological Properties of SCC to Predict Formwork Pressure," *Proceedings of SCC*, pp. 671-677.

Khayat, K., and Assaad, J., 2006, "Effect of *w/cm* and High-Range Water-Reducing Admixture on Formwork Pressure and Thixotropy of Self-Consolidating Concrete," *ACI Materials Journal*, V. 103, No. 3, pp. 186-193.

Khayat, K., and Assaad, J., 2008, "Use of Thixotropy-Enhancing Agent to Reduce Formwork Pressure Exerted by Self-Consolidating Concrete," *ACI Materials Journal*, V. 105, No. 1, pp. 88-96.

Khayat, K.; Assaad, J.; Mesbah, H.; and Lessard, M., 2005a, "Effect of Section Width and Casting Rate on Variations of Formwork Pressure of Self-Consolidating Concrete," *Materials and Structures*, V. 38, No. 1, pp. 73-78. doi: 10.1007/BF02480577

Khayat, K., and Omran, A., 2010a, "Evaluation of SCC Formwork Pressure," *Concrete International*, V. 32, No. 6, pp. 30-34.

Khayat, K., and Omran, A., 2010b, "State-of-the-Art Review of Form Pressure Exerted by Self-Consolidating Concrete," University of Sherbrooke, Sherbrooke, QC, Canada, 139 pp.

Khayat, K.; Omran, A.; and Pavate, T., 2010, "Inclined Plane Test to Evaluate Structural Buildup at Rest of Self-Consolidating Concrete," *ACI Materials Journal*, V. 107, No. 5, pp. 515-522.

Khayat, K.; Saric-Coric, M.; and Liotta, F., 2002, "Influence of Thixotropy on Stability Characteristics of Cement Grout and Concrete," *ACI Materials Journal*, V. 99, No. 3, pp. 234-241.

Khayat, K. H.; Petrov, N.; Assaad, J.; Morin, R.; and Thibault, M., 2005b, "Performance of SCC Used in Repair of Retaining Wall Elements," Proceedings 2nd North American Conference on the Design and Use of Self-Consolidating Concrete, S. P. Shah, ed., Chicago, Nov., pp. 1003-1012.

Koehler, E. P., and Fowler, D., 2004, "Development of a Portable Rheometer for Fresh Portland Cement Concrete," ICAR -105-3F, *International Center for Aggregates Research.* doi:10.15781/T2X539

Leemann, A., and Hoffmann, C., 2003, "Pressure of Self-Compacting Concrete on the Formwork," *3rd International Symposium on Self-Compacting Concrete*, pp. 288-295.

Matar, P., and Assaad, J., 2017, "Effect of Vertical Reinforcing Bars on Formwork Pressure of Scc Containing Recycled Aggregates," *Journal of Building Engineering*, V. 13, pp. 159-168. doi: 10.1016/j.jobe.2017.08.003

Mewis, J., 1979, "Thixotropy-a General Review," *Journal of Non-Newtonian Fluid Mechanics*, V. 6, No. 1, pp. 1-20. doi: 10.1016/0377-0257(79)87001-9

Mewis, J., and Wagner, N. J., 2009, "Thixotropy," *Advances in Colloid and Interface Science*, V. 147-148, pp. 214-227. doi: 10.1016/j.cis.2008.09.005

Omran, A.; Elaguab, Y.; and Khayat, K., 2014, "Effect of Placement Characteristics on SCC Lateral Pressure Variations," *Construction & Building Materials*, V. 66, pp. 507-514. doi: 10.1016/j.conbuildmat.2014.05.042

Omran, A., and Khayat, K., 2017a, "Effect of Formwork Characteristics on SCC Lateral Pressure," *Journal of Materials in Civil Engineering*, V. 29, No. 5, p. 04016293 doi: 10.1061/(ASCE)MT.1943-5533.0001827

Omran, A., and Khayat, K., 2017b, "Progress to Understand Influence of Reinforcement Density on SCC Lateral Pressure," *Materials and Structures*, V. 50, No. 2, p. 152 doi: 10.1617/s11527-017-1022-x

Omran, A.; Khayat, K.; and Elaguab, Y., 2012, "Effect of SCC Mixture Composition on Thixotropy and Formwork Pressure," *Journal of Materials in Civil Engineering*, V. 24, No. 7, pp. 876-888. doi: 10.1061/(ASCE)MT.1943-5533.0000463

Omran, A.; Naji, S.; and Khayat, K., 2011, "Portable Vane Test to Assess Structural Buildup at Rest of Self-Consolidating Concrete," *ACI Materials Journal*, V. 108, No. 6, Nov.-Dec., pp. 628-637.

Ovarlez, G., and Roussel, N., 2007, "A Physical Model for the Prediction of Lateral Stress Exerted by Self-Compacting Concrete on Formwork," *Materials and Structures*, V. 39, No. 2, pp. 269-279. doi: 10.1617/s11527-005-9052-1

Palacios, M., and Flatt, R. J., 2016, "Working Mechanism of Viscosity-Modifying Admixtures," *Science and Technology of Concrete Admixtures*, P.-C. Aïtcin and R. J. Flatt, eds., Woodhead Publishing, pp. 415-432.

Perrot, A.; Amziane, S.; Ovarlez, G.; and Roussel, N., 2009, "SCC Formwork Pressure: Influence of Steel Rebars," *Cement and Concrete Research*, V. 39, No. 6, pp. 524-528. doi: 10.1016/j.cemconres.2009.03.002

Prakash, N., and Santhanam, M., 2006, "A Study of the Interaction between Viscosity Modifying Agent and High Range Water Reducer in Self Compacting Concrete," *Measuring, Monitoring and Modeling Concrete Properties*, pp. 449-454.

Ritchie, A., 1962, "The Pressures Developed by Concrete on Formwork," *Civil Engineering and Public Works Review*, V. 57, No. 672, pp. 885-888.

Roby, H., 1935, "Pressure of Concrete on Forms," *Civil Engineering (New York, N.Y.)*, V. 5, No. 3, pp. 1-10.

Rodin, S., 1952, "Pressure of Concrete on Formwork," *Proceedings - Institution of Civil Engineers*, V. 1, No. 6, pp. 709-746. doi: 10.1680/iicep.1952.10980

Roussel, N.; Ovarlez, G.; Garrault, S.; and Brumaud, C., 2012, "The Origins of Thixotropy of Fresh Cement Pastes," *Cement and Concrete Research*, V. 42, No. 1, pp. 148-157. doi: 10.1016/j.cemconres.2011.09.004

Sperl, M., 2006, "Experiments on Corn Pressure in Silo Cells—Translation and Comment of Janssen's Paper from 1895," *Granular Matter*, V. 8, No. 2, pp. 59-65. doi: 10.1007/s10035-005-0224-z

Tattersall, G. H., and Banfill, P. F., 1983, *The Rheology of Fresh Concrete*, Pitman, 356 pp.

Tchamba, J.; Amziane, S.; Ovarlez, G.; and Roussel, N., 2008, "Lateral Stress Exerted by Fresh Cement Paste on Formwork: Laboratory Experiments," *Cement and Concrete Research*, V. 38, No. 4, pp. 459-466. doi: 10.1016/j.cemconres.2007.11.013

Tejeda-Dominguez, F.; Lange, D.; and D'Ambrosia, M., 2005, "Formwork Pressure of Self-Consolidating Concrete in Tall Wall Field Applications," *Transportation Research Record: Journal of the Transportation Research Board*, V. 1914, No. 1, pp. 1-7.

Vanhove, Y.; Djelal, C.; and Magnin, A., 2001, "A Prediction of the Pressure on Formwork by Tribometry," *American Society of Mechanical Engineers, Pressure Vessels and Piping Division*, V. 431, pp. 103-110.

Wallevik, J. E., 2003, "Rheology of Particle Suspensions: Fresh Concrete, Mortar and Cement Paste with Various Types of Lignosulfonates," The Norwegian University of Science and Technology, 411 pp.

Yamada, K.; Takahashi, T.; Hanehara, S.; and Matsuhisa, M., 2000, "Effects of the Chemical Structure on the Properties of Polycarboxylate-Type Superplasticizer," *Cement and Concrete Research*, V. 30, No. 2, pp. 197-207. doi: 10.1016/S0008-8846(99)00230-6

APPENDIX A—EXAMPLE CALCULATIONS

This appendix provides numerical examples to demonstrate how to use the various models and input parameters that are covered in Chapter 6. The calculated form pressure corresponds to the estimated pressure at the bottom of a

column that is 20 ft (6 m) in height. The casting rate and the density (unit weight) of the SCC are assumed to be 8 ft/h (2.4 m/h) and 144 lb/ft^3 (2306 kg/m^3), respectively. On the other hand, the concrete properties that are considered as input parameters for the various models are not the same. Therefore, the numerical examples do not yield the same maximum form pressure values.

A1—Calculation of form pressure using model by Gardner et al. (2012)

Inch-pound units
Height of column = 20 ft
Casting rate (R) = 8 ft/h
Total casting time (t_H) = 20/8 = 2.5 hours
Concrete density (unit weight) (w_c) = 144 lb/ft^3
Initial slump flow = 27 in.
Time to decrease the slump flow to 15.75 in. = 1.5 hours

Using Eq. (6.2a), time for the concrete slump to theoretically reach zero (t_0) can be computed as

$$t_0 = t_{15.75\text{ in.}}\left[\frac{\text{Initial slump flow (in.)}}{(\text{Initial slump flow (in.)} - 15.75)}\right]$$
$$= 1.5\left[\frac{27}{27-15.75}\right] = 3.6 \text{ hours}$$

Because t_H = 2.5 hours is less than t_0 = 3.6 hours, P_{max} is computed using Eq. (6.2b).

$$P_{max} = w_c R\left(t_H - \frac{t_H^{\,2}}{2t_0}\right) = 144 \times 8\left(2.5 - \frac{2.5^2}{2\times 3.6}\right) = 1880 \text{ psf}$$

SI units
Height of column = 6.1 m
Casting rate (R) = 2.44 m/h
Total casting time = 2.5 hours
Concrete density (unit weight) (w_c) = 2306 kg/m^3
Initial slump flow = 685 mm
Time to decrease the slump flow to 400 mm = 1.5 hours

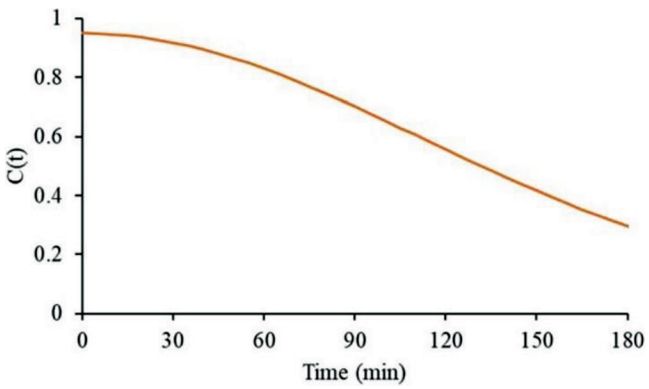

Fig. A1—Variations in C(t) *with time.*

Using Eq. (6.2a), time for the concrete slump to theoretically reach zero (t_0) can be computed as

$$t_0 = t_{400\text{ mm}}\left[\frac{\text{Initial slump flow (mm)}}{(\text{Initial slump flow (mm)} - 400)}\right]$$
$$= 1.5\left[\frac{685}{685-400}\right] = 3.6 \text{ hours}$$

Because t_H = 2.5 hours is less than t_0 = 3.5 hours, P_{max} is computed using Eq. (6.2b).

$$P_{max} = w_c g R\left(t_H - \frac{t_H^{\,2}}{2t_0}\right) = 2306 \times 9.81 \times 2.44\left(2.5 - \frac{2.5^2}{2\times 3.6}\right)$$
$$= 90{,}105 \text{ Pa} = 90.1 \text{ kPa}$$

A2—Calculation of form pressure using model by Khayat and Omran (2010b)

SI units
Height of the column = 6.1 m
Casting rate (R) = 2.44 m/h with no waiting period (that is, continuous casting)
Concrete density (unit weight) (w_c) = 2306 kg/m^3
Change in yield stress with rest time ($\tau_{0rest}(t)$) = 42.5 Pa/min
Yield stress measured after 15 minutes of rest ($\tau_{0rest@15min}$) = 758 Pa
Maximum size of the aggregate (MSA) = 20 mm
Diameter of the cross section (d) = 0.61 m
D_{min} = equivalent minimum form dimension. Based on Table 6.3a, for d > 0.5 m, D_{min} = 0.5 m
Based on Table 6.3b, for MSA 20 mm and $\tau_{0rest@15min}$ of 758 Pa, f_{MSA} = 1
Based on Fig. 6.3b, for continuous casting, f_{WP} = 1
Maximum lateral pressure exerted by SCC on the formwork (P_{max}) can be computed using Eq. (6.3).

$$P_{max} = \frac{w_c g H}{100}\left[95.9 - 3.84H + 0.71R + 4.1D_{min} - 0.29PV\tau_{0rest}(t)\right] \times f_{MSA} \times f_{WP}$$

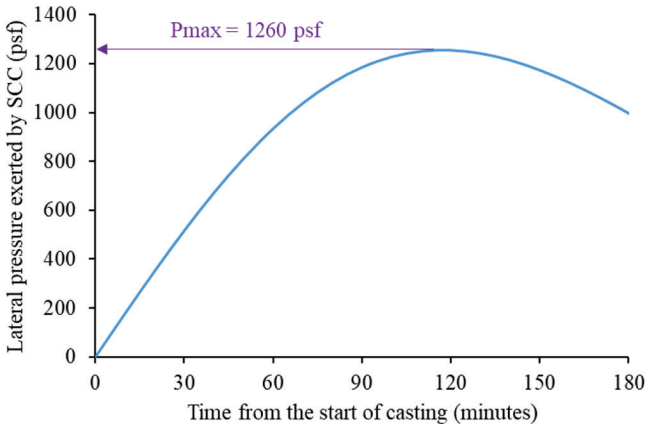

Fig. A2—Prediction of lateral pressure using the model by Tejeda-Dominguez et al. (2005).

$$P_{max} = \frac{2306 \times 9.81 \times 6.1}{100} \times \left[95.9 - 3.84(6.1) + 0.71(2.44) + 4.1(0.5) - 0.29(42.5)\right] \times 1 \times 1 = 88{,}224 \text{ Pa} = 88.24 \text{ kPa}$$

A3—Calculation of form pressure using model by Tejeda-Dominguez et al. (2005)

Inch-pound units
Height of the column = 20 ft
Casting rate (R) = 8 ft/h = 0.133 ft/min
Total casting time = 20/8 = 2.5 hour = 150 minutes
Temperature = 68°F
Concrete density (unit weight) (w_c) =144 lb/ft^3

The values of a, α, and C_0 are taken as $10^{-5.5}$, 12, and 0.95, respectively. These values were taken from Tejeda-Dominguez et al. (2005).

Using Eq. (6.4a), the decay function $C(t)$ can be computed as

$$C(t) = \frac{C_0}{(at^2+1)^{\alpha}} = \frac{0.95}{(10^{-5.5}t^2+1)^{12}}$$

The decay function $C(t)$ is shown in Fig. A1.

$$\text{Lateral pressure exerted by SCC} = (w_c Rt) \times C(t) = (144 \times 0.133 \times t) \times C(t) \text{ lb/ft}^2 = 19.152t \times C(t) \text{ psf}$$

The variation in the lateral pressure with time is shown in Fig. A2. The maximum pressure (P_{max}) is identified as 1260 psf. This function is maximized when:

$$t = \sqrt{\frac{1}{2a\alpha - a}} = \sqrt{\frac{1}{(2 \times 10^{-5.5} \times 12) - 10^{-5.5}}} = 117.3 \text{ minutes}$$

SI units
Height of the column = 6.1 m
Casting rate (R) = 2.44 m/h = 0.04 m/min

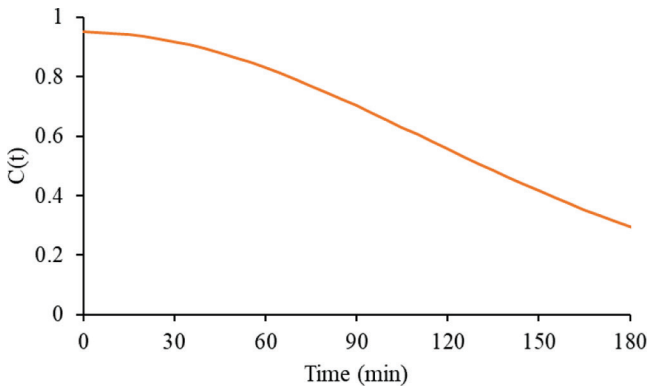

Fig. A3—Variation in C(t) *with time.*

Total casting time = 6.1/2.44 = 2.5 hours = 150 minutes
Temperature = 20°C
Concrete density (unit weight) (w_c) = 2306 kg/m^3

The values of a, α, and C_0 are taken as $10^{-5.5}$, 12, and 0.95, respectively. These values were taken from Tejeda-Dominguez et al. (2005).

C_0 = 0.95 (typical value for the tests run in the lab)

Using Eq. (6.4a), the decay function $C(t)$ can be computed as

$$C(t) = \frac{C_0}{(at^2+1)^{\alpha}} = \frac{0.95}{(10^{-5.5}t^2+1)^{12}}$$

The decay function $C(t)$ is shown in Fig. A3.

$$\text{Lateral pressure exerted by SCC} = (w_c gRt) \times C(t) = (2306 \times 9.81 \times 0.04 \times t) \times C(t) = 904.87t \times C(t) \text{ Pa} = 0.9t \times C(t) \text{ kPa}$$

The variation in the lateral pressure with time is shown in Fig. A4. The maximum pressure (P_{max}) is identified as 60.1 kPa. This function is maximized when:

$$t = \sqrt{\frac{1}{2a\alpha - a}} = \sqrt{\frac{1}{(2 \times 10^{-5.5} \times 12) - 10^{-5.5}}} = 117.3 \text{ minutes}$$

A4—Calculation of form pressure using model by Ovarlez and Roussel (2007)

Inch-pound units
Height of the column = 20 ft
Casting rate (R) = 8 ft/h
Concrete density (unit weight) (w_c) =144 lb/ft^3
Change in yield stress with rest time ($\tau_{0rest}(t)$) = 53.3 psf/h
Diameter of the cross section (e) = 2 ft

Horizontal or lateral pressure exerted by SCC on the formwork (P_H) can be computed using Eq. (6.5).

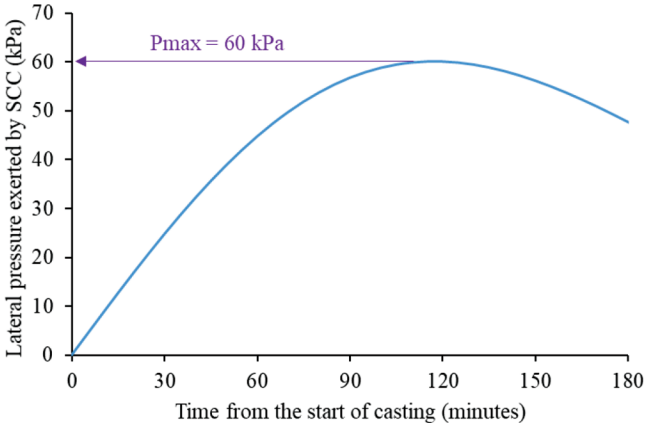

Fig. A4—Prediction of lateral pressure using the model by Tejeda-Dominguez et al. (2005).

$$P_{max}\,(\text{psf}) = w_c H\left(1-\frac{H\tau_{0rest}(t)}{w_c eR}\right)$$

$$= 144\times 20\left(1-\frac{20\times 53.3}{144\times 2\times 8}\right) = 1550 \text{ psf}$$

SI units

Height of the column = 6.1 m

Casting rate (R) = 2.44 m/h

Concrete density (unit weight) (w_c) =2306 kg/m^3

Change in yield stress with rest time ($\tau_{0rest}(t)$) = 42.5 Pa/min = 2550 Pa/h

Diameter of the cross section (e) = 0.61 m

Horizontal or lateral pressure exerted by SCC on the formwork (P_H) can be computed using Eq. (6.5).

$$P_{max}\,(\text{Pa}) = w_c gH\left(1-\frac{H\tau_{0rest}(t)}{w_c geR}\right)$$

$$= 2306\times 9.81\times 6.1\left(1-\frac{6.1\times 2550}{2306\times 9.81\times 0.61\times 2.44}\right)$$

$$= 72{,}240 \text{ Pa} = 72.2 \text{ kPa}$$

American Concrete Institute
Always advancing

As ACI begins its second century of advancing concrete knowledge, its original chartered purpose remains "to provide a comradeship in finding the best ways to do concrete work of all kinds and in spreading knowledge." In keeping with this purpose, ACI supports the following activities:

- Technical committees that produce consensus reports, guides, specifications, and codes.
- Spring and fall conventions to facilitate the work of its committees.
- Educational seminars that disseminate reliable information on concrete.
- Certification programs for personnel employed within the concrete industry.
- Student programs such as scholarships, internships, and competitions.
- Sponsoring and co-sponsoring international conferences and symposia.
- Formal coordination with several international concrete related societies.
- Periodicals: the ACI Structural Journal, Materials Journal, and Concrete International.

Benefits of membership include a subscription to Concrete International and to an ACI Journal. ACI members receive discounts of up to 40% on all ACI products and services, including documents, seminars and convention registration fees.

As a member of ACI, you join thousands of practitioners and professionals worldwide who share a commitment to maintain the highest industry standards for concrete technology, construction, and practices. In addition, ACI chapters provide opportunities for interaction of professionals and practitioners at a local level to discuss and share concrete knowledge and fellowship.

American Concrete Institute
38800 Country Club Drive
Farmington Hills, MI 48331
Phone: +1.248.848.3700
Fax: +1.248.848.3701

www.concrete.org

American Concrete Institute
Always advancing

38800 Country Club Drive
Farmington Hills, MI 48331 USA
+1.248.848.3700
www.concrete.org

The American Concrete Institute (ACI) is a leading authority and resource worldwide for the development and distribution of consensus-based standards and technical resources, educational programs, and certifications for individuals and organizations involved in concrete design, construction, and materials, who share a commitment to pursuing the best use of concrete.

Individuals interested in the activities of ACI are encouraged to explore the ACI website for membership opportunities, committee activities, and a wide variety of concrete resources. As a volunteer member-driven organization, ACI invites partnerships and welcomes all concrete professionals who wish to be part of a respected, connected, social group that provides an opportunity for professional growth, networking and enjoyment.

9 781641 951449